J Mater Sci (2024) 59:14948–14980

Review

Review of scientific literature and standard guidelines for the characterization of graphene-based materials

Thais Alves[1,2], Wanessa S. Mota[2], Cecília Barros[4], Danilo Almeida[3], Daniel Komatsu[4], Aleksandra Zielinska[5,6], Juliana C. Cardoso[7], Patrícia Severino[2], Eliana B. Souto[5,*], and Marco V. Chaud[1,*]

[1] *Laboratory of Biomaterials and Nanotechnology (LaBNUS), University of Sorocaba - UNISO, University City Campus, Raposo Tavares, Sorocaba, São Paulo 18023-000, Brazil*
[2] *Institute of Technology and Research (ITP), University of Tiradentes (UNIT), Aracaju, Sergipe 49010-390, Brazil*
[3] *School and College of Technology SENAI – Santos Dumont, São José Dos Campos, São Paulo 12212-100, Brazil*
[4] *Laboratory of Biomaterials, Pontificial University Catholic (PUC), Sorocaba, SP 18030-070, Brazil*
[5] *Laboratory of Pharmaceutical Technology, Faculty of Pharmacy, University of Porto, Jorge de Viterbo Ferreira, 4050-313 Porto, Portugal*
[6] *Institute of Natural Fibers and Medicinal Plants National Research Institute, ul. Wojska Polskiego 71b, 60-630 Poznań, Poland*
[7] *Postgraduate Program in Health and Environment, Tiradentes University, Aracaju, Sergipe 49032-490, Brazil*

Received: 28 March 2024
Accepted: 26 July 2024
Published online: 2 August 2024

© The Author(s), 2024

ABSTRACT

Graphene is a two-dimensional carbon material with unique properties, such as high thermal and electrical conductivity, mechanical strength, elasticity, and biocompatibility. The methods used to synthesize graphene affect its structural properties, including flaws, layer count, crystalline domain size, and impurities, ultimately affecting the properties and performance of graphene-based materials. This review aims to analyze the methods used to characterize graphene, using both ISO/IEC standards and current literature as references. The discussed techniques are diverse, yet complementary, and include ultraviolet–visible spectroscopy, Raman spectroscopy, X-ray photoelectron spectroscopy, Fourier transform infrared spectroscopy, X-ray diffraction, X-ray absorption near edge structure, atomic force microscopy, scanning electron microscopy, transmission electron microscopy, the Brunauer–Emmett–Teller method, thermogravimetric analysis, in-line four-point probe, resonant cavity and terahertz time-domain spectroscopy, besides an alternative method to determine the graphene domain. By employing rigorous characterization techniques, researchers and industry professionals can ensure the reliability, effectiveness, and trustworthiness of graphene-based materials for various applications.

Handling Editor: Annela M. Seddon.

Address correspondence to E-mail: ebsouto@ff.up.pt; marco.chaud@prof.uniso.br

https://doi.org/10.1007/s10853-024-10061-4

Introduction

In the late 2000s, techniques for characterizing graphene gained significant prominence. However, in the fifteen years that followed, only about 300 narrative reviews on graphene characterization techniques were published in journals with a reasonable impact factor. Over the last five years, there has been a significant increase in publications addressing graphene physicochemical characterization, due to diverse applications of this material in different fields of knowledge. However, the use of different techniques for the same purpose results in distinct outcomes for graphene, graphene oxide and graphene reduced, which may have led to a biased interpretation of the results.

Graphene can be described as a two-dimensional (2D) allotrope of carbon, composed of a single layer of densely packed sp^2-bonded atoms of carbon arranged in a honeycomb-shaped crystal lattice [1]. Graphene, graphene oxide (GO), and reduced GO (rGO) are receiving great attention from researchers in different areas of science as novel nanomaterials with superior physical properties [2–5]. These properties include their (i) biocompatibility; (ii) thermal conductivity, (iii) electrical conductivity, (iv) mechanical strength, and (v) surface-to-volume ratio [6–8].

For graphene synthesis, two main methods, namely top-down and bottom-up—are proposed. In top-down synthesis methods, graphite is broken down into graphene; by contrast, in bottom-up synthesis methods, graphene is obtained from decomposing carbon-containing precursors, both liquid and gaseous, producing graphene layers with a hexagonal structure [9, 10]. Each of the methods used in graphene synthesis prints its fingerprint on the structure, namely, flaws in the crystalline lattice, the size of the crystalline domains, the number of layers, and the substituting impurities [9]. Table 1 lists the advantages and limitations of various bottom-up and

Table 1 Advantages and limitations of the methods commonly used for the synthesis of graphene

Synthesis route	Number of layers	Advantages	Limitations
Top-down methods			
Mechanical exfoliation	Mono/Multiple layers	High quality Simple process Uniform size Large size area Low cost	Low yield Non-scalable
Liquid phase exfoliation (LPE)	Mono/Multiple layers	High quality Scalable Low cost Short time	Nonuniform flakes Low yield of monolayer Small size Long time
Electrochemical exfoliation	Multiple layers	High quality Scalable Low cost Short time	Slight oxidation Requires ionic liquids High cost
Arc discharge	Mono/Multiple layers	Low cost High quality Environmentally friendly	Low yield Presence of carbonaceous impurities
Bottom-up methods			
Chemical vapor deposition (CVD)	Mono/Multiple layers	Large size area Scalable Choice of carbon precursors Excellent conductivity High quality	High cost Complex process
Epitaxial growth (SiC)	Multiple layers	Low defects No substrate transfers Perfect integration High quality	High cost Uncontrolled size

top-down methods used in the synthesis of graphene [7, 11].

The properties of graphene and its potential applications depend on the following three key parameters: (i) the number of layers; (ii) the distance between layers; and (iii) impurities (mainly oxygen compounds and oxides) [7]. Thus, characterization techniques play a significant role in understanding and evaluating graphene properties. By employing these characterization techniques, researchers and industry professionals can ensure quality control, optimize performance, validate synthesis methods, and detect fraud, ultimately contributing to the advancement and utilization of graphene in various applications. The International Organization for Standardization (ISO) published several technical specifications (TS) and technical reports (TR) about graphene nomenclatures, properties, and characterizations. Moreover, the International Electrotechnical Commission (IEC) publishes standard techniques for graphene characterization (IEC/TS 62607) [12].

The informative ISO/TS 80004-13:2017 [13] reports the definitions and terms for graphene and its related 2D materials, besides properties, characterization and methods for production. In 2020, ISO/TS 80004-3:2020 was published [14], in which the terms related to carbon nano-structures were defined. The ISO/TR 19733:2019 [15] covers the critical properties of graphene and its related 2D materials, as well as the commercially available techniques for the assessment and measurement of their physical, chemical, electrical, thermal, mechanical and optical properties. In 2021, the ISO/TS 21356-1:2021 was published, covering the structural characterization of graphene in form of powders and liquid dispersions [16]. This standard guideline describes the measurement techniques and provides a decision-making process for the understanding of the structural properties of graphene particles, in powder form or as liquid dispersions (Fig. 1).

In this review, a study of graphene has been conducted, aiming at providing a guidance regarding the relevant characterization techniques, according to ISO/IEC standards, to mitigate the risk of biased interpretation of results. These techniques can be employed to investigate the morphology, properties, flaws, number of layers, and conductivity of graphene. Various methods are examined, including ultraviolet–visible spectroscopy (UV–vis), Raman spectroscopy, Fourier transform infrared spectroscopy (FT-IR), X-ray photoelectron spectroscopy (XPS), X-ray diffraction (XRD), X-ray absorption near edge structure (XANES), AFM, SEM, TEM, the BET method, thermogravimetric analysis (TGA), in-line four-point probe (4PP), resonant cavity and terahertz time-domain spectroscopy (THz-TDS), and also describing an alternative method to

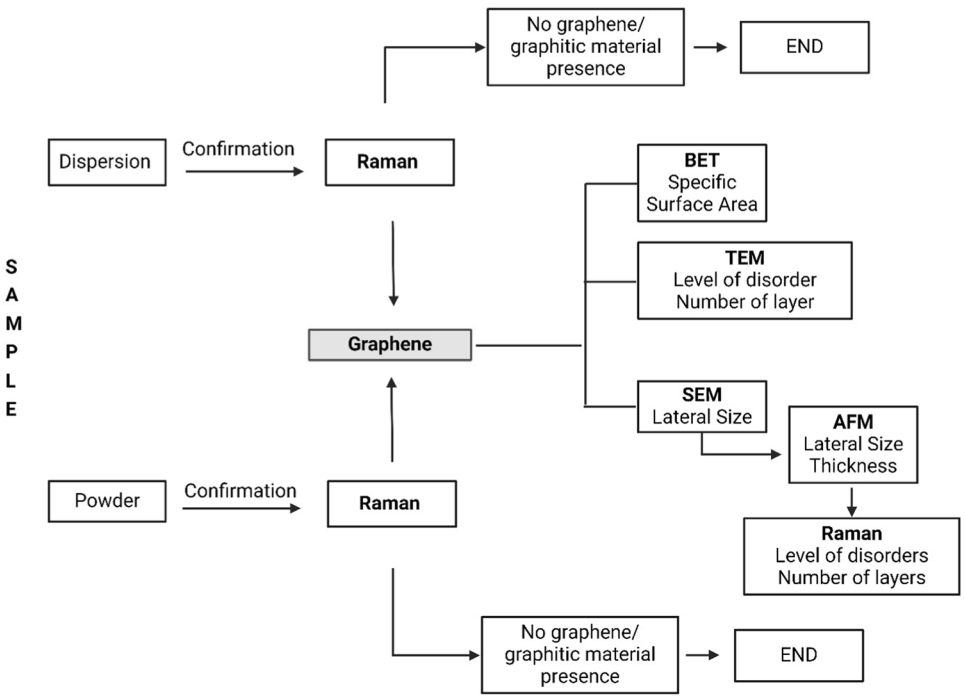


Figure 1 Decision-making process to determine the structural properties of graphene from a powder or a liquid dispersion, according to ISO/TS 21356-1:2021.

determine the graphene domain according to the ISO/IEC standards.

Methodology

In this study, the protocol for reviewing the literature consisted of (i) a search process, (ii) study selection followed by analysis, and (iii) reporting. The search process was conducted using Boolean operators and descriptors, such as graphene, graphene oxide, and reduced graphene oxide characterization; graphene synthesis route; graphene AND "analysis name" (ultraviolet–visible spectroscopy, Raman spectroscopy, Fourier transform infrared spectroscopy, etc.); graphene ISO standard; and graphene IEC. The information about the characterization and application of graphene was collected from articles published over the last 5 years. The libraries used to search were Google Scholar, Science Direct, PubMed, Scopus, Springer, Web of Science, American Chemical Society (ACS), Taylor and Francis, Wiley Online Library, ISO, and IEC standards.

The literature research was screened and filtered based on the title, abstracts, and contents, to respond to the aim of our review. The information and data underwent a thorough analysis and were presented in various forms, such as discussions, figures, tables, and graphics.

Characterization of graphene

The characterization of graphene is a crucial aspect of its research. It involves the analysis of the material's morphology, properties, defects, and layers. Table 2 summarizes the essential techniques for characterizing graphene, their applications, and their limitations, as outlined in ISO/IEC standard documents and current literature. The subsequent sections explore how to apply and interpret the results of each technique used to characterize graphene.

Ultraviolet–visible spectroscopy

UV–vis spectroscopy is a useful technique for characterizing various types of graphene, such as pristine graphene, GO, and few-layer graphene. The absorption observed in the UV–vis spectra arises from electron transitions that occur at the carbon π bonds. The $\pi - \pi^*$ electronic transition (~ 230 nm), an electron transitions from the π bonding molecular orbital to the corresponding π * anti-bonding molecular orbital. This phenomenon is observed in graphene oxide (GO) samples, which pertains to the dispersion of electrons within the π bonding network across the graphene plane [29]. On the other hand, the $n - \pi^*$ electronic transition (~ 300 nm) involves the excitation of an electron from a non-bonding orbital (n) to the anti-bonding π^* orbital. In GO samples, this transition is associated with oxygen-containing functional groups on the graphene surface. Such transitions can induce alterations in the electronic structure of the graphene lattice, thereby affecting the material's electronic and optical properties [1, 17–19]. In general, the literature does not address the method for preparing an aqueous dispersion of graphene, GO, or rGO for UV–vis analysis. However, ISO/TS 21356-1:2021 [16] proposes the use of the sonication method, where the graphene sample is prepared by its dispersion in deionized water and shaken for 10 min with an ultrasonic device at a power of 120 W and a frequency of 40 Hz.

A new approach for obtaining few-layer graphene from graphite flakes was developed. The method uses ethanol in the exfoliation technique, without the need for high boiling point solvents, surfactants, or polymers. A notable peak at approximately 269 nm was observed, which corresponds to π–π* transitions of graphene and graphite (Fig. 2a) [50]. Moreover, the concentration of dispersed graphene was determined using the Beer–Lambert equation (Eq. 1), where the absorbance (A) is the concentration (c) of the dissolved substance and the optical path length (l) of the sample. The (α) absorption coefficient is a constant and can be considered a measure of the electronic transition of substance [51].

$$A = \alpha . c . l \tag{1}$$

When GO is reduced to produce rGO, the absorption peak of GO observed at approximately 230 nm shifts to approximately 260 nm, suggesting a repair in π-conjugated assemblies (aromatic structure) [19, 51, 52].

In a green approach to synthesizing GO, citric acid was employed to reduce GO instead of using toxic sodium nitrate ($NaNO_3$), furthermore, the washing steps were simplified, and the overall time required for the synthesis of GO and rGO was reduced [53]. The authors used UV–vis spectroscopy to validate the

Table 2 Summary of graphene characterization techniques

Technique	Application	Limitation	References
Ultraviolet–visible spectroscopy (UV–vis)	Plasmonic sensing capability; Investigates the degree of graphene oxidation; Differentiates graphene from graphene oxide (GO; 262 nm and 230 nm, respectively)	Analyzed in solution medium; Possibility of cluster formation	[1, 17–19]
Raman spectroscopy	Investigates the graphene structure quality, defects, and number of graphene layers; Nondestructive technique; Deformation and mechanical properties of carbon materials	Small signals; Difficulty to develop robust and trustworthy quantitative data analysis methods	[20–24]
Fourier transform infrared spectroscopy (FT-IR)	Determines the presence or absence of functional groups on GO or reduced GO	Not frequently recommended for the detection of the presence of metallic species in graphene or GO The broad spectrum should be checked—spectrum overlapping	[10, 18, 25]
X-ray photoelectron spectroscopy (XPS)	Surface analysis technique; Informs about the quantitative composition with respect to the elements, their chemical and electronic state on graphene surface; Determines the amount of oxygen on graphene and GO; Nondestructive technique	Analyzes of films with a thickness > 10 nm	[25–27]
X-ray diffraction (XRD)	Provides qualitative properties such as crystallinity degree and fingerprints; Helps to differentiate between graphite and graphene; Determines the interplanar spacing of the atomic planes in graphene material; Estimates the exfoliation degree; Nondestructive technique	Not suitable for identifying single-layer graphene	[22, 27–29]
X-ray absorption spectroscopy (XAS)	Detects the unoccupied states in conduction bonds; Elucidates the electronic properties of materials	Minimum concentration limits for samples	[8, 25, 30, 31]
Scanning electron microscopy (SEM)	Surface roughness; Lateral dimensions; Detects impurities, folds, and discontinuities; Images are in the order of mm × mm with a depth of field in the order of mm; Nondestructive technique	Limited resolution for ultrathin graphene layers	[14, 22]

Table 2 continued

Technique	Application	Limitation	References
Transmission electron microscopy (TEM)	Provides the morphological properties and number of layers of graphene (a single or few layers); HRTEM[1] offers a high magnification and high resolution down to a single atom or group of atoms; Nondestructive technique	Slow	[21, 22, 32]
Atomic force microscopy (AFM)	Provides information about the following: Thickness; Number of layers: Lateral dimensions; Surface roughness; Flake thickness; Lattice mismatch; Cutting of graphene; Mechanical properties; Electrical properties; Nondestructive technique	Lateral resolution sensitive to the sharpness of tip; Slow scanning	[8, 22, 33–35]
Brunauer–Emmett– Teller (BET) method	Evaluates the surface area and porous size, including for powders; Measurements of gas adsorption	Only dry powders; Not applicable to all types of isotherms; Exhibits variation between measurements	[10, 36, 37]
Thermogravimetric analysis (TGA)	Tool for the qualitative and quantitative analysis of graphene materials; Identifies “fake graphene”; Determines the thermal stability; Indicates the removal of oxygen-containing groups from GO and the formation of reduced GO	Destructive technique	[36, 38, 39]
In-line four-point probe (4PP)	Standard technique; Measures sheet electric resistance; Highest measurement accuracy; No special sample preparation is required	Destructive technique; Contact technique	[40–42]
Resonant cavity	Measures surface conductance; non-contact; non-destructive	Applied to materials synthesized by CVD on metal substrates, epitaxial growth on silicon carbide, obtained from rGO, or mechanically exfoliated from graphite	[43–46]

Table 2 continued

Technique	Application	Limitation	References
Terahertz time-domain spectroscopy (THz TDS)	Spatially maps electrical properties; Measures the conductivity in a large area of graphene sheet; Noncontact technique; Non-destructive technique	Inhomogeneity of the substance surface, opacity, and high atmospheric humidity (during measurement) lead to low efficiency of this method	[40, 47–49]

[1]HRTEM: high-resolution transmission electron microscopy

proposed method to investigate the profile transition of graphene, GO, and rGO (Fig. 2b). In Fig. 2b, the black line in the spectrum of GO exhibits two absorption peaks, one at 233 nm and a shoulder peak at 304 nm. The presence of these peaks was attributed to the transitions in C–C bonds (π–π^*) and the C = O (n–π^*) of GO sample, respectively. Moreover, when comparing the absorption peaks of GO and rGO (red line), the peak at 233 nm in GO sample was changed to 263 nm in rGO sample, indicating a repairing in π-conjugated assemblies (aromatic structure) [53].

Raman spectroscopy

Raman spectroscopy is a highly effective, nondestructive technique that characterizes various types of carbon materials, including crystalline, nanocrystalline, and amorphous carbons [8, 20].

The Raman effect results from molecules or solids inelastic scattering of photons. When a photon interacts with a molecule or a solid, this may cause a change in the energy state of the molecule or solid, resulting in the emission of a scattered photon with a different wavelength. The high resolution and sensitivity to C–C bond vibration allow Raman spectroscopy to provide information about the optical, electronic, and phonon properties of carbon materials [20].

IEC/TS 62607-6-14:2020 establishes a standardized method to determine the defect level for powders of graphene-based material by Raman spectroscopy [54]. The sample should be prepared by putting the graphene powder on a flat substrate and then pressing it with a glass slide to obtain a tablet (thick enough so that Raman signals from the substrate can be neglected). The measurements should be carried out at room temperature under dark ambient conditions.

In Raman Spectroscopy, graphene can be characterized using various excitation wavelengths from visible lasers, such as 633 nm, 532 nm, or 785 nm [55]. However, IEC/TS 62607-6-14:2020 establishes that the wavelength of the laser can be 514 nm, 532 nm, and 633 nm [54], and the incident power density of the laser should be 0.4 mW/μm^2 to 1.2 mW/μm^2 (to avoid burning the sample). The square scan area should be 10 × 10 μm, with a minimum of five points for each sample. The spectral range is chosen such that the relevant Raman bands appear in a single spectrum to reduce the measurement time.

The Raman spectra of the graphene samples show three main distinctive peaks: (i) G-band, (ii) D-band,

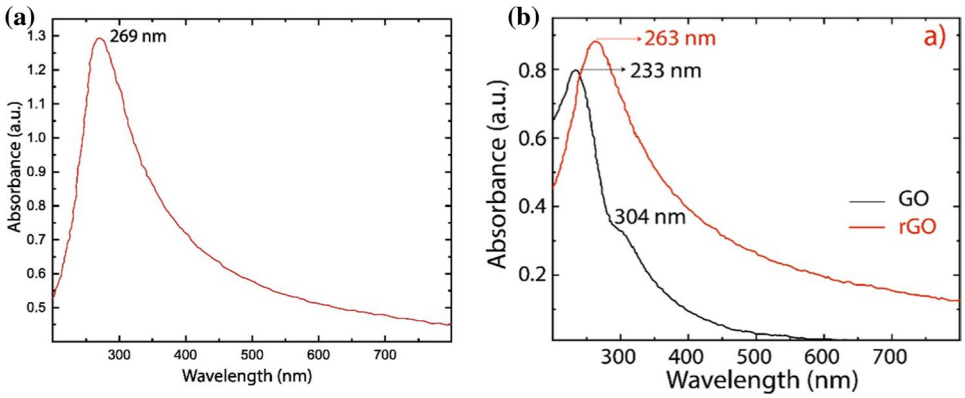


Figure 2 **a** UV–visible spectra of graphene (Reproduced with permission from reference [50]. Copyright 2021, Elsevier). **b** UV–visible spectra recorded in aqueous solutions of GO (black line) and rGO (red line) (Reproduced with permission from reference [53]. Copyright 2020, The Authors).

and (iii) 2D-band. The G-band is a vibrational mode associated with sp^2-bonded carbon atoms in a crystalline lattice, i.e., it represents the level of structural order. The D-band is associated with disorders and defects, or the mode is close to an edge in the graphene structure. The 2D-band is an overtone of the D-band, and its peak shape can indicate the layer thickness. Thus, it is possible to obtain semi-quantitative parameters of the quality of graphene samples through of ratio between D- and G-band intensities (ID/IG), where a higher value of I_D/I_G indicates a higher degree of disorder or defects in the material, while a lower value indicates a more ordered or crystalline material [8, 21, 22, 56].

To interpret the results according to IEC/TS 62607-6-14:2020 [54], it is necessary to obtain a background baseline by fitting the spectrum without bands, and the data should be processed by peak fitting techniques. Moreover, before the analysis of the defect level, the sample should be analyzed by the 2D-band signal to determine its layer structure. In case the ratio between the main band and shoulder band is larger than 1.25, the data will not be appropriate for analysis of defect level, due to the possible presence of graphite structure.

A representative Raman spectrum of the produced graphene, along with bulk graphite for comparison, is displayed in Fig. 3a, where the D-band (~ 1350 cm^{-1}), G-band (~ 1580 cm^{-1}), and 2D-band (~ 2700 cm^{-1}) are indicated [57]. Zhang et al. [57] observed an intensity ratio of D/G (I_D/I_G) of 0.1 for the prepared graphene, thereby confirming the high quality of the obtained graphene.

In a study by Childres et al. [58], Raman spectroscopy was used to analyze graphene samples produced with predetermined levels of defects, caused by exposure to electron-beam irradiation and oxygen plasma etching. The technique was conducted using a 532-nm excitation laser. Figure 3b depicts the disorder induced in graphene by the electron-beam exposure. The D-band intensity increased with the increasing irradiation dosage, which indicates the enhanced disorder of the graphene. Furthermore, the I_D/I_G ratio increased from 0.3 at 50 e^-/nm^2 to 4 at 10000 e^-/nm^2, before decreasing to 3.7 at 30000 e^-/nm^2, indicating a transition into the high-disorder level [58].

Raman spectroscopy has also been used to determine the number of graphene layers in flakes, as illustrated in Fig. 4a and b. The most widely used fingerprint for monolayer graphene is probably an I_{2D}/I_G ratio of more than 3. Thus, with the increased number of layers of a monolayer to seven layers, the 2D-band's shape changes, and the intensity ratio of I_{2D}/I_G bands decreases. For instance, with an increasing number of layers, the peak position of the 2D-band shifts to higher numbers. Figure 4c and d illustrate that the D-band's intensity increases with the number of layers, while the intensity ratio of I_{2D}/I_G bands decreases [23, 59].

The effectiveness of Raman Spectroscopy has been demonstrated in the study of the mechanical properties and deformation behavior of graphene materials with high resolution at the micro-scale. Deformations change both the bond length and energy, which can be characterized by measuring the down-/up-shift rate of the Raman band position per % strain. Graphene materials typically exhibit linearly elastic band shift rates, expressed in terms of stress rather than strain. Usually, D, G, and 2D bands exhibit

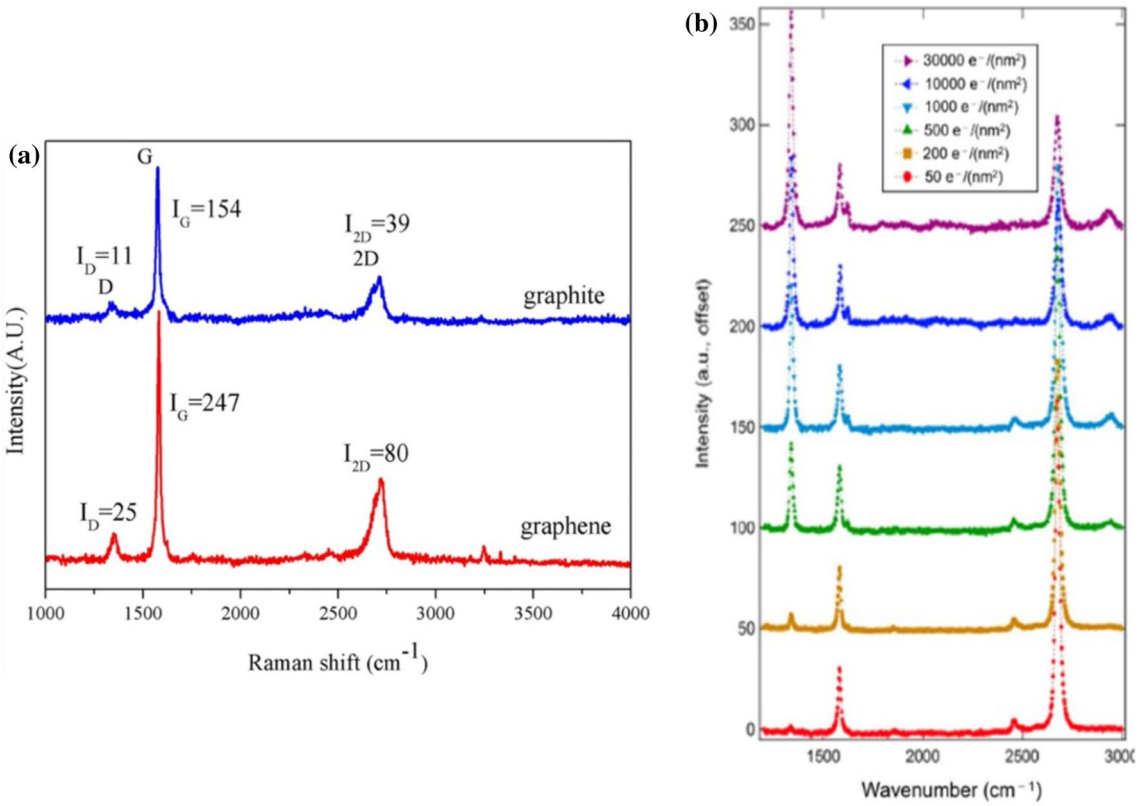


Figure 3 **a** Raman spectroscopy of bulk graphite and graphene (Reproduced with permission from reference [57]. Copyright 2018, The Authors). **b** Raman spectra (excitation wavelength 532 nm) of graphene (Adapted with permission from reference [58]. Copyright 2022, The Authors).

similar trends, but their different vibrational modes result in distinct shifts and broadening rates [23, 60].

IEC/TS 62607-6-6:2021 establishes a standardized approach to determine, by Raman spectroscopy, the strain uniformity for single-layer graphene [61]. Some requirements are necessary to obtain these data, such as: (i) There is no need for any specific preparation of the sample; (ii) the sample should be placed on insulating surfaces and certain metals (e.g., copper), (iii) the sample should be significantly larger than the size of the Raman laser spot, (iv) the substrate material should not obscure the D-, G-, and 2D peaks of the graphene sample, (v) tt is advisable to use a laser power below 1 mW to prevent any thermal effects, (vi) the achieved spot size (FWHM) in confocal mode must be less than 1 μm, and (vii) it is advised to have a spectral resolution of at least 1.5 cm^{-1}. Raman spectroscopy can be used to directly determine the stacking order of graphene samples. Specifically, the 2D peak exhibits a symmetric line shape only in single-layer graphene.

The Raman spectroscopy maps should be recorded in confocal mode, where the system scans. The maps are taken over a square scan area of 10 μm × 10 μm. The guidelines suggest utilizing a configuration that allows for the measurement of all Raman peaks in a single image capture, thereby minimizing the time required for the measurement After scanning the graphene sample and recording a full Raman spectrum for each spot, the acquired data is further processed by standard peak fitting techniques using *Lorentzians* fits. From the fits, the peak position, integrated intensity, and FWHM are extracted for every spectrum. The next step is to plot FWHM (2D) as a 2D map.

Graphene micro-ribbons were produced by the bottom-up method (chemical vapor deposition) using UV photolithography and dry-etching oxygen plasma treatments [62]. These graphene micro-ribbons were incorporated into a polymeric matrix poly (methyl methacrylate) and subjected to tension and compression. The analysis used an Argon ion laser (514.5 nm), a diode laser (785 nm), and laser power below 0.25

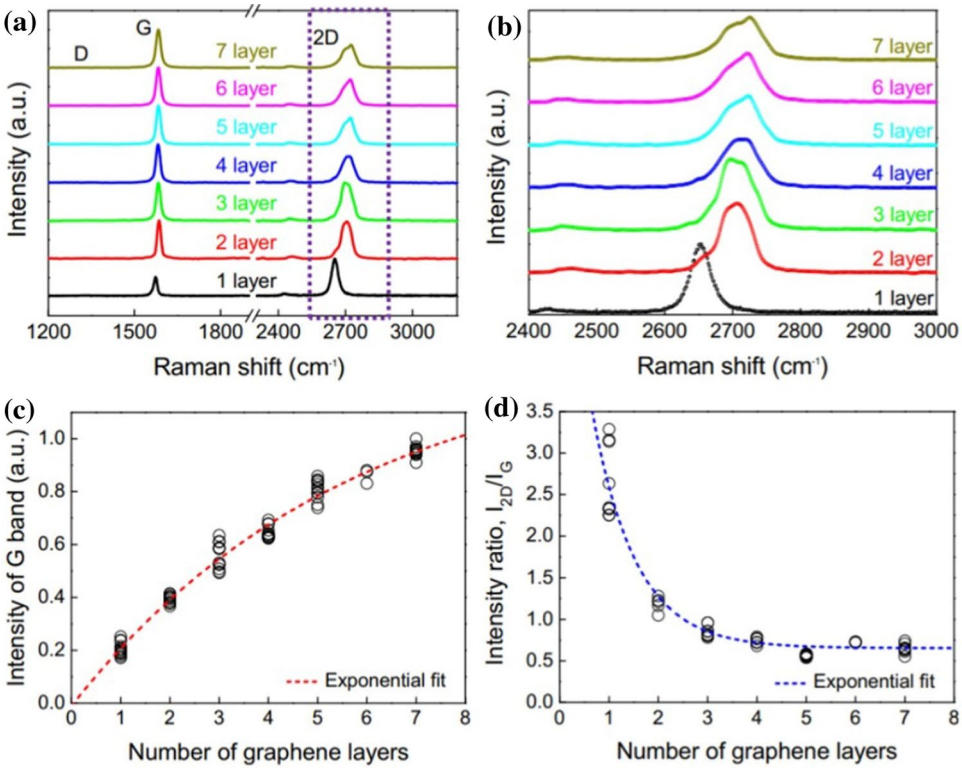


Figure 4 Raman spectra of one- to seven-layered graphene: **a** and **b** spectral evolution; **c** intensities of G-bands; and **d** intensity ratios I_{2D}/I_G graphene (Reproduced with permission from reference [59]. Copyright 2014, Elsevier).

mW. Moreover, uniaxial tensile (steps of 0.1%) and compressive (steps of 0.5%) loadings were applied to graphene micro-ribbons embedded into the PMMA, by a cantilever beam technique [62]. Figure 5a and b display the representative Raman spectra of graphene at various strain levels in the G-bands and 2D-bands. Meanwhile, Fig. 5c and d exhibit the G and 2D band fitted versus of strain, respectively.

Under tension, the authors observed that both the 2D-bands and G-bands exhibited a linear behavior for strain (indicated by the red lines), with − 14.8 cm^{-1}/% for the 2D-band, and − 5.7 cm^{-1}/% for the G-band. On the other hand, under compression, both bands exhibited a nonlinear tendency for strain, with + 12.3 cm^{-1}/% for the 2D-band and + 5.1 cm^{-1}/% for the G-band (values based on the linear portion of the graph—indicated by the red lines) [62].

Fourier transform infrared spectroscopy

Fourier transform infrared spectroscopy (FTIR) is a commonly used as an effective technique for characterizing materials based on GO by identifying residual functional groups. However, it is not suitable for detecting metallic species on the surface of GO materials, nor pure graphene because it does not produce signals. The IEC/TS 62607-6-18:2022 establishes that a FTIR spectrum can be obtained by ATR measurement for graphene samples [63]. The graphene powder should be deposited on the ATR base and be gently pressed with a glass slide.

The intense vibrational peak at 3425 cm^{-1} is attributed to the O–H stretching of water molecules. The absorption peaks at 1718 and 1632 cm^{-1} can be attributed to stretching modes of –C = O of –COOH and –C = C, respectively. Other strong and intense vibrational bands can be observed at 1373, 1222, and 1054 cm^{-1}, referring to the stretching modes of C–O–C (epoxy), tertiary C–OH, and C–O (alkoxy) groups, respectively [10, 64]. Whijaya et al. [64] studied the ecofriendly reduction of GO using the aqueous extract of *Kaffir lime* peels as a reduction agent of graphene. Figure 6a shows the functional groups of graphite, GO, and rGO.

FTIR analysis of graphite revealed the presence of C = C groups in graphite at 1512.08 cm^{-1}. The oxidation of graphite was confirmed by the spectrum of GO, which showed peaks at 3656.54 cm^{-1} (O–H); 1704.73 cm^{-1} (C = O); 1090.23 cm^{-1} (= CH); and 1382 cm^{-1} (C-O).

The reduction of GO was confirmed by the restoring of the aromatic group (C = C), peaks at 1,456 cm^{-1} and

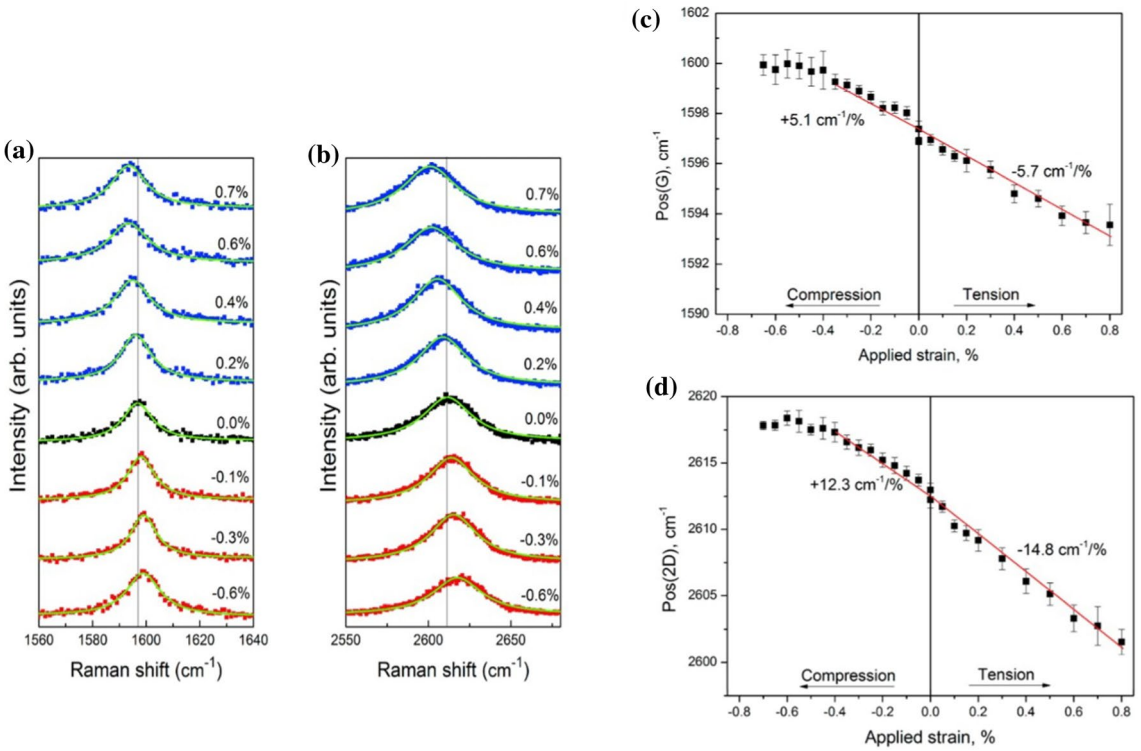


Figure 5 **a** Evolution of the G-bands and **b** 2D-bands versus strain for micro-ribbons incorporated in polymeric matrix. The blue points indicate under tension test and red points indicate under compression test. **c** Position of G-band and **d** 2D-band versus strain, which solid lines represent tendency to the experimental results (Reproduced with permission from reference [62]. Copyright 2019, The Authors).

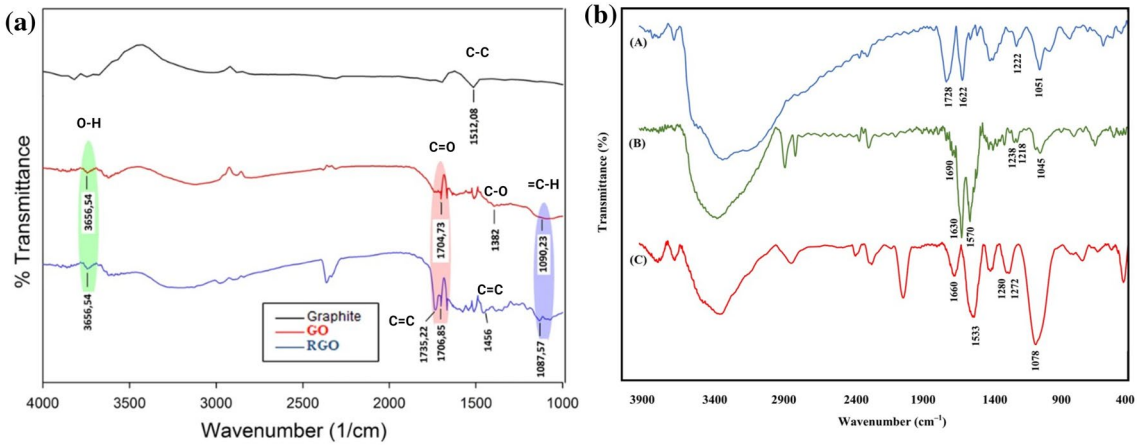


Figure 6 **a** FT-IR spectra of graphite, GO, and rGO (Reproduced with permission from reference [53]. Copyright 2020, The Authors). **b** FT-IR spectra of GO (**a**), GO-FA (**b**), and GO-FA/SF nanobiocomposite scaffold (**c**) (Reproduced with permission from reference [65]. Copyright 2022, The Authors).

1735.22 cm^{-1}, as seen in the rGO spectrum. The remaining C = O group (1706.85 cm^{-1}) in the rGO spectrum indicates a partial reduction of GO [64]. Additionally, various other functional groups can be easily detected in GO-based materials by FTIR. For instance, the presence of alcoholic and phenolic groups can be

identified through their O–H stretching absorption at 3590–3650 cm^{-1}, while amines can be detected through N–H stretching vibrations at 3300–3500 cm^{-1}. Bands at 1700–1750 cm^{-1} indicate the presence of amides, which have C = O bonds adjacent to N. Thio compounds, on the other hand, can be detected through C–S or C = S vibrations at 616 cm^{-1}, 1070 cm^{-1}, and 1423 cm^{-1} [10].

Nanocomposite scaffolds based on silk fibroin incorporating GO (produced by the Hummers' method), covalently functionalized with folic acid, were produced and evaluated by FTIR in the region 400–4000 cm^{-1}, using KBr pellets [65]. The synthetic GO spectrum (Fig. 6B-a) exhibited a broad band between 3400 and 3350 cm^{-1} assigned to the hydroxyl groups (–OH). The bands at 1728 and 1622 cm^{-1} were assigned to the stretching vibration of the carboxyl group (C = O) and unoxidized graphitic domain (C = C), respectively. Additionally, small stretching of alcohol groups (C–OH) and epoxy or alkoxy groups (C–O) were observed at 1222 and 1051 cm^{-1} [65].

In the GO–FA spectrum (Fig. 6B-b), characteristic peaks of GO were observed at 1630, 1238, and 1045 cm^{-1}, corresponding to C = C, C–OH, and C–OR groups. In addition, the authors also reported peaks referring to amide bond formation during folic acid conjugation at 3470–3320 cm^{-1} (N–H); in the range 3470–3320 cm^{-1} (N–H); at 1570 cm-1 (C–N); and 1218 cm^{-1} (aliphatic amine group) [65].

A quantitative approach to evaluate the degree of oxidation of different GO samples can be made by calculating the relative percentage of oxygen-containing functional groups (RP). It is calculated by the ratio between the sum of the area of all peaks area of C = C peak, and the sum of the area of all peaks multiplied by 100 (Eq. 2) [66]:

$$RP = \left(\frac{\text{Sum of area of all peaks area of C = C peak}}{\text{Sum of area of all peaks}}\right) * 100 \quad (2)$$

An alternative method to FTIR analysis is its coupling with TGA analysis. It is used to identify and quantify functional groups (e.g., hydroxyl, amino, carboxyl, alkyl, carbonyl, sulfonic acid group) in graphene powder. The volatilization and pyrolysis cause the sample weight loss, which is quantitatively monitored by TGA. The evolved gas from the TGA is transferred by purge gas flow in line and reaches the gas cell of FTIR in the sample compartment, where the spectrum is measured. This method is described in the IEC/TS 62607-6-18:2022 [63].

To perform the analysis, the IEC/TS 62607-6-18:2022 suggests using the tableting sample of graphene with a mass of at least 5 mg [63]; TGA temperature from 25 °C to 1200 °C; heating rate of 5 °C min^{-1}; and purifying with nitrogen or helium at a 50 mL.min^{-1} flow rate. The temperature of the gas cell and transfer line should be held at 300 °C and 280 °C, respectively. For FTIR, the spectrum scope is 400 cm^{-1} to 4000 cm^{-1} with a resolution factor of 8 cm^{-1}. After analysis, it is possible to obtain the TGA curve (weight loss temperatures), as well as the 3D FTIR spectrum (intensity versus wavenumber versus time or temperature).

X-ray photoelectron spectroscopy

XPS provides valuable information about the elemental composition (detection sensitivity of 0.1–1 at % for all elements except H and He), chemical state (oxidation state, functional groups, and bonding configurations), electronic structure (Fermi-level position, doping level, and band structure modifications), surface properties (surface roughness and the presence of defects or surface contaminants), and the amount of oxygen in graphene samples [25–27]. The number of defects can be analyzed by the O/C ratio, quantifying different carbon functionalities, identifying chemical bond formations, and evaluating the physisorption (i.e., physical adsorption) of molecules. IEC/TS 62607-6-21:2022 establishes a standardized method to determine the elemental composition, and C/O ratio by XPS for graphene powders samples, namely, graphene, bi- and tri-layer graphene, few-layer graphene, graphene nanoplate, GO, rGO, and functionalized graphene powders [67].

The guideline suggests that the sample is in pellet form, but if a pellet cannot be produced, a similar continuous sample should be prepared to avoid any signal from the mounting substrate. The sample is transferred to the XPS, and a vacuum pumping is carried with a pressure lower than 5×10^{-8} mbar. The scan is performed over an energy range of 0 to 1000 eV, the counts per second (CPS) value at C 1 s peak should be no less 1×10^5.

The high-resolution scan is performed at the range of C 1 s, O 1 s, N 1 s, Cl 2p, and S 2p peaks, with a pass energy of 40 eV and the scanning step should be set from 0.05 eV to 0.1 eV. To obtain a high-quality signal, the sample should be scanned so that the peak intensity is greater than 2×10^4 counts for the C 1 s peak. At the same time, the other peaks should be

scanned for the same scanning number as the C 1 s. The measurement should be conducted with two or three parallel samples and in five different positions for each.

There are two methods for calculating the O/C ratio, namely, (i) the area method, and (ii) the fitting method [68].

The area method is a direct and accurate approach for calculating the O/C ratio; however, it has limitations when external sources of oxygen signals are present. To ensure the accuracy of the O 1 s peak, measurements must be conducted on graphene samples deposited on oxygen-free substrates, such as clean Au, or on relatively thick GRM samples (> 15 nm). Using SiO_2, a common substrate in electronics applications, can introduce artefacts and hinder the direct calculation of O/C_{area}. Moreover, interpreting O 1 s spectra can be challenging due to their broad nature and multiple overlapping components, as well as the difficulty in distinguishing between the substrate and deposited graphene sample contributions. Therefore, the focus is on the quantitative analysis of C 1 s surveys conducted to address these challenges [68].

The fitting method is applicable to all substrates and sample thicknesses; however, it often introduces systematic and intrinsic errors due to the employed fitting procedure. The fitting method involves deconvoluting the C 1 s signal into its several components, such as defects (sp^3), graphitic carbon (sp^2), carbons bonded to carbonyl and carboxyl groups, or hydroxyl and epoxy groups. Thus, using these deconvoluted C 1 s signals, it is possible to calculate the O/C ratio (O/C_{fit}), without using the oxygen peak [68].

IEC/TS 62607-6-21:2022 was established for graphene powder samples; however, the literature describes the technique for graphene aqueous dispersion. Foschi et al. (2021) [69] tested pristine GO and rGO (thermally reduced) for the removal of triazines from water. The GO/rGO samples were fabricated through drop-casting an aqueous dispersion (1.0 mg/mL, 50 µL in volume) onto a gold substrate. XPS spectra were gathered under ultra-high vacuum settings using a pass energy of 11.75 eV, resulting in an experimental resolution of 0.25 eV. The obtained XPS spectra were fitted employing Voigt line shapes and Shirley backgrounds.

Through XPS analysis (Fig. 7a), the researchers determined the percentage of C 1 s and O 1 s peaks, which allowed them to estimate the C/O ratio. For GO, the calculated C/O ratio was found to be 1.99, indicating a high degree of oxidation in the material. The calculated C/O ratio for rGO at 110 °C was 2.51. This value was slightly higher than that of the oxidized sample since some of the oxygenated groups were cleaved, resulting in a higher carbon-to-oxygen ratio [69].

The initial GO sample shows the presence of a high number of oxygenated groups, confirmed by the relative area percentages of 53.7%, 35.1%, and 11.3% for C–C, C–O, and C = O, respectively. However, upon analysis of the deconvoluted peaks, the authors observed that, in the reduced sample treated at 110 °C, the contribution of C–C increased from 53.7% to 57.8%. Simultaneously, the C–O signal became wider, and its intensity was reduced, thus decreasing the ratio of O/C_{fit} from 35.1% to 30.9%. This information corroborated the partial reduction of GO [69].

X-ray diffraction

XRD is a technique that creates a diffraction pattern from the atoms within a crystal lattice with the application of X-rays. In addition, the generation of three-dimensional images that demonstrate the electron densities within the crystals is allowed by the pattern established from the intensities and angles of the diffracted X-rays [29]. This technique is widely used to provide relevant information about the type of graphene material and its structural characteristics, including defects, crystal orientation, lattice parameters, and stacking order [8, 22].

IEC/TS 62607-6-17:2023 establishes a standardized method to determine the typical order parameter for graphene-based material and layered carbon material (graphite, expanded graphite, amorphous carbon, vitreous carbon, glassy carbon, and reduced graphene oxide) by XRD and TEM [70]. However, the graphene oxide is not within the scope of this guideline. This technical specification suggests the preparation method for graphene samples, where an amount of powder sample should be deposited in the groove of the sample loader and then pressed with a glass slide so that the sample surface is as flat as possible, following the cover of the center of the groove.

In addition to the standardized method, the literature describes the use of XRD to characterize GO powder and films. The X-ray diffractogram of graphite depicts two characteristic peaks, one at $2\theta = 26°$ ($d_{002} = 0.34$ nm) and other at $2\theta = 55°$ ($d_{004} = 0.17$ nm),

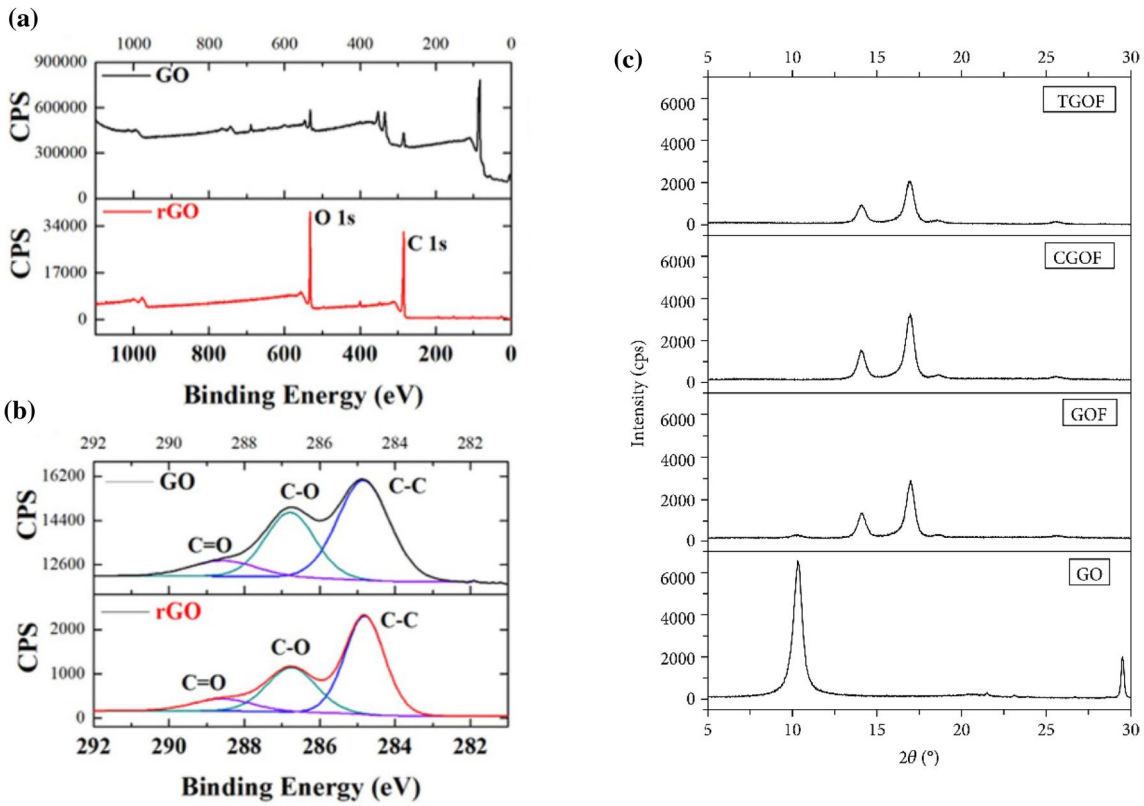


Figure 7 **a** XPS spectrum of GO (black line) and rGO (red line) at 110 °C, **b** C 1 s region of GO (black line) and rGO (red line) (Reproduced with permission from reference [69]. Copyright 2021, The Authors). **c** X-ray diffractograms of powder GO, GO film (GOF), chemically rGO film (CGOF), and thermally rGO film (TGOF) (Reproduced with permission from reference [28]. Copyright 2019, The Authors).

while the GO sample has a diffraction peak at 2θ = 10°, corresponding to a layer-to-layer distance of 0.88 nm. The increase in interlayer spacing of GO is attributed to the functionalization with oxygen-containing groups [28, 71]. Furthermore, studies also describe that the reduction of GO to rGO can be confirmed by shift of the diffraction peak. The diffraction peak of GO at 2θ = 10° shifts to 2θ = 23.8°, corresponding to a layer-to-layer distance of 0.37 nm. The lower values of interlayer spacing of rGO, than of GO, occur due to the removal of oxygen-containing functional groups, resulting in the restacking of rGO sheets [8, 72].

Reduced graphene oxide produced by Gascho et al. [28] was evaluated to determine the most effective technique for obtaining high-quality rGO (chemical or thermal), and later film production. For XRD analysis, the samples were mounted on an amorphous silicon sample holder for analysis using parameters, such as a 2θ angle spanning from 5 to 70° and a wavelength of 1.5406 Å, operating at 40 kV and 30 mA.

In the X-ray diffractogram of GO presented in Fig. 7c, only a single peak is observed at 2θ = 10° (d002 = 0.84 nm), confirming the effectiveness of the oxidation reaction of graphite. However, after the formation of the films (GOF), new peaks at 2θ = 14° (d_{002} = 0.63 nm), 2θ = 17° (d_{002} = 0.52 nm), 2θ = 19° (d_{002} = 0.48 nm) were identified, and in lower intensity at 2θ = 26° (d_{002} = 0 34 nm), referring to the remaining graphite. After the reduction of GO (chemical-CGOF, or thermal -TGOF), the same peaks were observed, indicating a partial reduction of the GO. The authors highlighted that the peaks seen in the analysed GO materials have not yet been referenced by others [28].

X-ray absorption spectroscopy

XAS is a technique that provides detailed information about the transitions from the core electronic states of the material to its excited electronic states [30]. It is a comprehensive technique that comprises the X-ray fluorescence (XRF) and X-ray absorption fine spectroscopy (XAFS) which, in turn, includes X-ray absorption near-edge structure (XANES or NEXAFS) and extended X-ray absorption fine structure (EXAFS) [73].

To understand the electronic structure around the C and O atoms and their local hybridization in the GO and rGO sheets, Sharma et al. [74] and [75] performed XANES spectra at O K-edge and C K-edge. The C K-edge XANES spectra presented in Fig. 8a indicate that the graphite, GO, and rGO samples exhibit three main spectral features at 285.3–288.5 (1 s → π* transitions) and 291–293 eV (1 s → σ* transitions). The higher intensity of these features for graphite sample was observed because of the larger number of sp^2 hybridized carbon atoms. By contrast, the GO and rGO samples show a reduced intensity of these three spectral features, which suggests a decrease in the number of sp^2 hybridized carbon atoms [74, 75]. Similar results

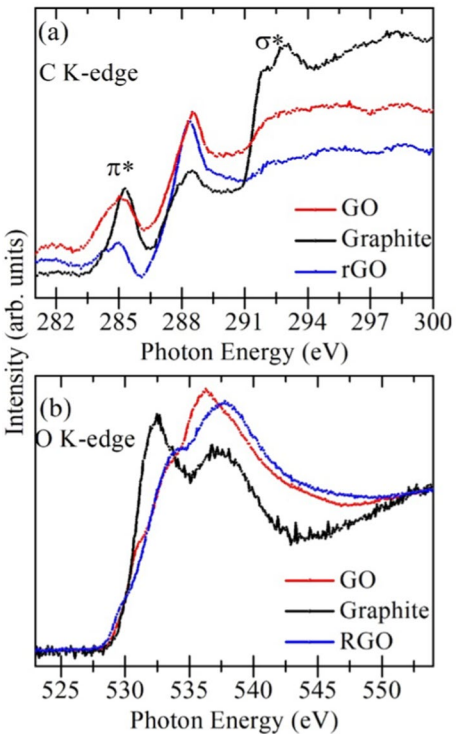


Figure 8 **a** CK-edge and **b** OK-edge spectra of graphite, GO, and rGO (Reproduced with permission from reference [75]. Copyright 2019, The Authors).

were obtained by Ganya et al. [31] in their study about the variations in electronic and magnetic properties of the polyacrylate-grafted GO/r-GO nanocomposites.

The O K-edge XANES spectra of graphite, GO, and rGO samples are presented in Fig. 8b. They exhibit two spectral features in the range between 530 and 550 eV. In the graphite samples, it is possible to see the first feature next to 532.2 eV, and the second between 535 and 545 eV. The low energy feature is associated with the transition of the O 1 s → C = O π* from the carbonyl groups bonded with the edge sides of the aromatic ring, while the high energy feature (535–545 eV) is associated with the transition of the O 1 s → O–H σ*, C–O σ* and C = O σ*, from groups hydroxyl, carbonyl, and carboxylic acid bonded in the aromatic ring. On the opposite, the GO and rGO samples exhibit a lower intensity in the first spectral feature and have a shoulder feature at 533 eV. Moreover, a higher intensity in the second spectral feature for GO and rGO was observed, highlighting the attachment of additional oxygen groups in the aromatic ring [74, 75].

Scanning electron microscopy

SEM uses a focused beam of electrons to scan sample surfaces and, through the interaction of these electrons with atoms, it generates high-resolution, high-magnification images [8, 22].

ISO/TS 21356-1:2021 recommends preparing the graphene sample by dispersing it in deionized water (or isopropanol) and submitting it to stirring for 10 min using an ultrasonic machine set at a power of 120 W and a frequency of 40 Hz [16]. Subsequently, 10–1000 µl of the dispersed mixture should be placed onto a support grid (silicon dioxide substrate) and subjected to vacuum for 2 h or longer at 40 °C to reduce solvent residue. The gold powder can be used to cover the sample. The equipment must be configured for an acceleration voltage less than or equal to 5 kV, and images with low magnification (~ 10000× magnification) should also be obtained for the areas containing the graphene flakes. Furthermore, it is suggested to collect and analyze the image of more than 200 flakes, selected randomly to measure the lateral size of the flake. The result of flake lateral size can be plotted in a 20-bar histogram.

Figure 9 presents SEM images of graphite, GO, and rGO. In Fig. 9b, changes in morphology are noted, where a reduction in the bulk density of GO occurs compared to graphite (agglomerate powder—many

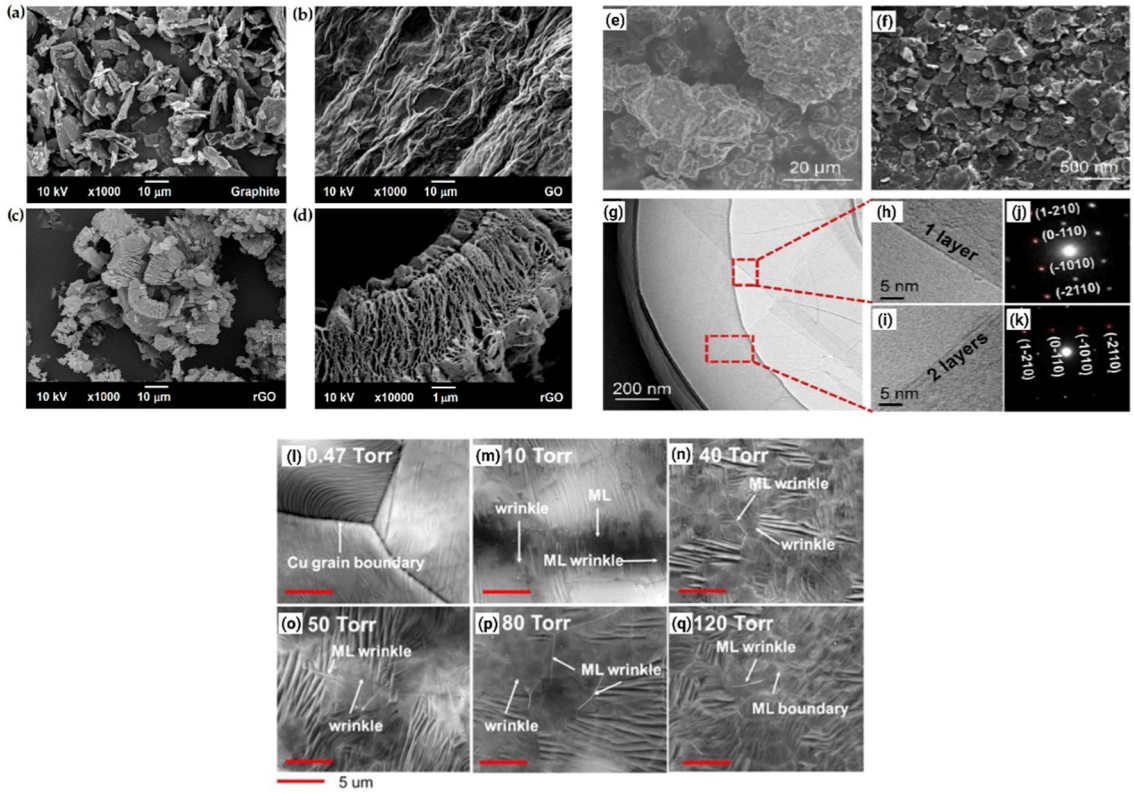


Figure 9 SEM images of (**a**, **e**) graphite; (**b**) graphene oxide; and (**c**, **d**) reduced graphene oxide (Reproduced with permission from reference [76]. Copyright 2021, The Authors). SEM images ESfG (**f**); Low- (**g**) and high-resolution (**h**, **i**) TEM images, the selected area's electron diffraction patterns (**j**, **k**) of h, I (Reproduced with permission from reference [77]. Copyright 2021, Elsevier). SEM images of graphene grown on copper foil at (**l**) 0.47, (**m**) 10, (**n**) 40, (**o**) 50, (**p**) 80, and (**q**) 120 Torr, where ML is an abbreviation for multilayer. The scale bar indicates 5 µm (Reproduced with permission from reference [78]. Copyright 2019, The Authors).

graphene layers; Fig. 9a). GO exhibits a smooth surface with wrinkles and folded regions, due to the presence of oxygen-containing functional groups and structural defects (Fig. 9b) [76]. During the oxidation–reduction process in the production of rGO, the layers of graphite were exfoliated, resulting in a coarse-grained agglomerate powder (Fig. 9c and d). The thermal reduction process caused micro-explosions, leading to the formation of a porous structure in rGO, with gases released and pores formed between graphene layers. Different oxidation and reduction conditions did not significantly affect the morphology of individual rGO samples, but all resulted in the formation of a porous product [76]. Ding et al. [77] introduced a straightforward method for synthesizing sulfonic acid functionalized graphene (ESfG) with edge selectivity. They employed a combination of SO_3 gas-assisted mechano-chemical exfoliation and high-yield synthesis techniques using graphite as the starting material. The SEM images presented in Fig. 9e depict the pristine graphite powder, which is stacked with each other, showing smooth edges and a lateral size exceeding 20 µm. On the contrary, the exfoliated ESfG showed surface feathery, lamellar morphologies, and a lateral size smaller than graphite (Fig. 9f).

The monolayer graphene can be produced using Cu substrate by the CVD method; however, its efficiency is limited to the production of bi- or multilayer graphene. The Cu is a catalyst for graphene synthesis, and when the surface is covered by graphene, new layers are stopped to grow. Cho et al. [78] studied the graphene growth in bi and multilayers using the CVD method associated with Cu substrate and hydrogen partial pressure controlled. Figure 9l–q display a sequence of SEM images that illustrate the graphene growth on copper foil at different pressures: 0.47, 10, 40, 50, 80, and 120 Torr. The graphene grown at 0.47 Torr (Fig. 9l) exhibits a smooth monolayer

without wrinkles, with only copper steps visible on the graphene surface [78].

Under higher-pressure conditions (Fig. 9m–q), the authors described the presence of bright white wrinkles in the graphene samples, suggesting the formation of a graphene multilayer. While the wrinkles in monolayer graphene appeared in a darker contrast [78].

Transmission electron microscopy

TEM uses the transmission of an electron beam through a fragile specimen, typically with a thickness of less than 100 nm. Thus, TEM enables the acquisition of high-resolution images that can reveal atomic-level details. It finds extensive applications in determining the number of graphene layers within a flake. Furthermore, it is possible to use high-resolution transmission electron microscopy (HRTEM) and high-resolution scanning transmission electron microscopy (HRSTEM) to provide the highest structural information available, allowing for a fundamental characterization of graphene samples at the atomic level [21, 22].

IEC/TS 62607-6-17:2023 establishes a standardized method to determine the typical order parameter for graphene-based material and layered carbon material [70]. The recommended procedure for preparing the graphene sample involves dispersing it in absolute ethanol and submitting it to stirring for 15 min using an ultrasonic machine set at a power of 120 W and a frequency of 40 Hz. Then 2 µl of dispersed mixture should be dropped onto a support grid and left to dry naturally for one hour before TEM measurement.

In addition, ISO/TS 21356-1:2021 focuses on structural characterization employing TEM, encompassing measurements of lateral size, number of layers, and alignment between layers of graphene flakes [16]. In cases where the lateral sizes of the flakes exceed 3 µm, it becomes impractical to measure the lateral size of 200 representative flakes. Therefore, only the number of layers and alignment between layers of graphene flakes should be analyzed. Samples must be prepared by dispersing graphene flakes in solvent and shaking until complete dispersion, then a volume of 100–200 µL must be deposited on the TEM grid. Then, the sample must be dried at ~ 150 °C under vacuum for 8 h. The TEM must be set to a resolution of at least 0.2 nm, with an accelerating voltage less than or equal to 80 kV.

Reduced graphene oxide was produced using an *Eclipta prostrata* phytoextract by the infusion method and, to evaluate the variation in the stacking characteristics, graphite, GO, and rGO were analyzed using TEM. A small quantity of sample in aqueous dispersion form was deposited on a copper grid and covered with thin amorphous carbon film, then the sample was dried using a vacuum desiccator. TEM images of graphite displayed increased folding and wrinkling. At the same time, the GO sample showed a relatively flat structure with low contrast, indicating a thickness of only a few graphene layers and sharp edges. After reduction by *E. prostrata* aqueous extract, TEM images revealed that the rGO sheets developed lattice fringes with smooth edges and transparent sheets [79].

Navik et al. [80] examined the morphology of few-to-multi-layer graphene using TEM, where the aqueous dispersion samples were deposited on a standard carbon/Cu grid, and dried in a vacuum oven at 40 °C for 24 h. Their study revealed that, within the analyzed graphene flakes, approximately 70% consisted of few-layer graphene, while the remaining 30% consisted of multi-layer graphene. The authors provided HRTEM images that showcased exfoliated graphene sheets that resulted from the exfoliation process. These images exhibited large, transparent graphene flakes, primarily composed of few-layer graphene [80].

TEM and HRTEM were used to characterize the crystal morphology and to determine the layer number of sulfonic acid functionalized graphene (ESfG) nanosheets obtained through exfoliation. Figure 9g–k present both low- and high-resolution TEM images as well as a selected area electron diffraction pattern. The TEM images reveal that the ultrathin ESfG nanosheets exhibited a nearly transparent appearance with crumpled morphologies, as depicted in Fig. 9g. Through HRTEM, Ding et al. [77] were able to clearly identify single- and bi-layer ESfG based on their edge structures, as depicted in Fig. 9H–I. Moreover, the intensity of electron diffraction spots provided a definitive means of identifying the layer number of ESfG (Fig. 9j–k). Typically, the diffraction intensity of the (0–110) plane was stronger for single-layer ESfG, while the (1–210) plane exhibited a stronger intensity for bi- or tri-layer ESfG [77].

Atomic force microscopy

AFM is a highly valuable technique for studying graphene at the nanoscale, providing a three-dimensional representation of data whereas images captured by SEM and TEM are typically bidimensional [81]. Its high resolution, reaching sub-angstrom levels, enables the distinction of single atomic layers on a substrate. This makes it ideal for characterizing film quality, including morphology, roughness, and uniformity [34, 82].

Furthermore, the AFM technique involves physical contact between a probe and the surface, allowing for the simultaneous determination of electrical (surface potential, electrostatic charge, and magnetic fields) and mechanical properties (stiffness, viscoelasticity, adhesion, deformation, Young's modulus, and friction) alongside the topography with nanoscale lateral precision. The probe's contact occurs in the film center, where a load is applied and generates a flexural deformation, and information on elasticity is measured to obtain the force–displacement curve. The provided elasticity measurements can reach values of hundreds of GPa when a diamond scanning probe is used. To determine Young's modulus, two Hertzian mechanical models, namely the Johnson–Kendall–Roberts and Derjaguin–Muller–Toporov models, can be employed [33, 35, 83, 84].

ISO/TS 21356-1:2021 focuses on measuring the lateral size and thickness by AFM analysis for graphene flakes [16]. The sample should be prepared as described in Item 3.7. This guide suggests that AFM measurements should be performed on materials where the lateral flake size distribution has previously been determined using SEM analysis.

A suitable AFM probe compatible with intermittent contact mode should be chosen, and the oscillation frequency should be shifted from the center of the resonance peak by 5% of the full width at half maximum (FWHM) value. Typical parameters for the probe are spring constant ~ 40 N/m, resonance frequency 240 kHz, and apex size between 5 and 15 nm. Initially, it is advisable to scan an area of 20 μm × 20 μm, with a scan speed of 10 μm/s and a resolution of 256 pixels × 256 pixels. Next, a smaller area scan of 2 μm × 2 μm is suggested, with a resolution of 512 pixels × 512 pixels. Analysis must be carried out for at least 20 graphene flakes.

Nanosized carbon materials are attractive for tissue engineering, due to their mechanical and electrical properties. GO is a "hydrophilic derivative" of graphene with low electrical conductivity, but it can support cell attachment, growth, and differentiation without cytotoxic effects [85, 86]. Pilato et al. [87] developed a 3D scaffold using GO flakes for cardiac repair applications. They reported to be the first time that a 3D structure of GO was produced using layer-by-layer interfaces employing the covalent growth of multilayer architectures of GO sheets alternated with linear macromolecules (polyethyleneimine), in a controlled way. Morphological features of the GO scaffold were obtained by AFM and SEM analyses, and Young's modulus was measured using the peak force quantitative nanomechanical mapping (PFQNM) mode of AFM. To analyze topography properties, a scan size area of 10 μm × 10 μm was performed using a frequency 300 kHz, and nominal elastic constant of 40 N/m. In PQNM analysis, probes with a nominal spring constant of 200 N/m and a resonance frequency of 525 kHz were applied [87].

The results revealed distinct characteristics for different samples. In the case of GO_1 and GO_1–PEI samples, isolated GO sheets were clearly observed on the surface (Fig. 10A and B). The height cross-sectional profiles of monolayer GO ($GO_{1)}$ showed the existence of GO sheet with a thickness between 1.68 and 1.76 nm, whereas the roughness of the flakes caused brighter ripples.

The GO_1–PEI network displayed a slightly larger thickness compared to GO_1 (1.54–1.68 nm), which was attributed to the presence of the amine PEI crosslinker. Furthermore, the GO_2 (two layers GO) and GO_5 (five layers GO) samples exhibited uniformly covered surfaces with GO–PEI networks, resulting in 3D architectures with maximum thicknesses of 70 nm and 130 nm, respectively (Fig. 10C and D), showing a proportional increase with the number of incubations [87].

The PFQNM mode analysis provided a detailed map of the samples' nanomechanical properties, allowing for the measurement of indicators, such as deformation and Young's elastic modulus. For the GO2 sample, Young's modulus was 20.9 ± 4.4 GPa and deformation of 1.30 ± 0.38 nm (Fig. 10F), while for the GO5 sample, Young's modulus was 12.9 ± 3.1 GPa and deformation of 1.99 ± 0.57 nm (Fig. 10E). The requested deformation could not be achieved for both GO1-PEI and GO1 samples, due to their high stiffness [87].

Among the information obtained through AFM, the determination of the sheet size of graphene is critical for the production and application of graphene-based

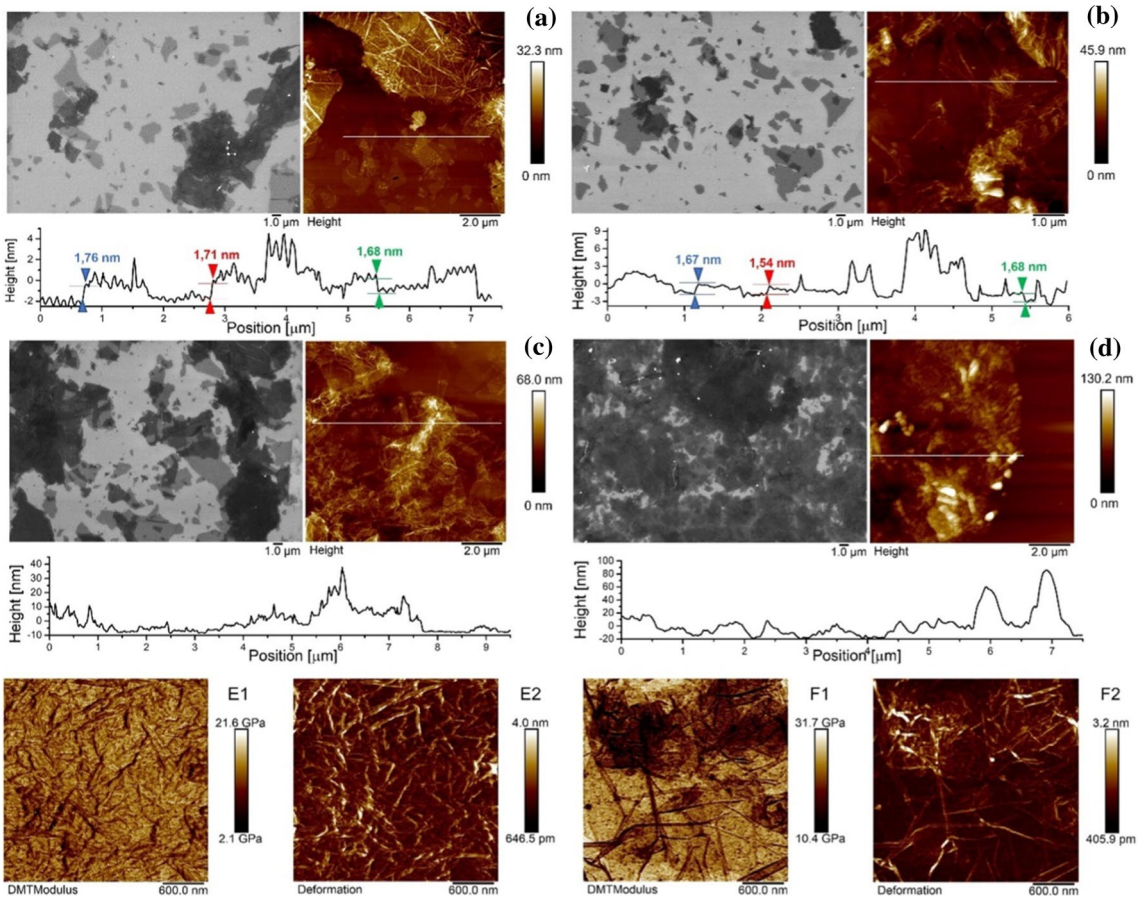


Figure 10 SEM, AFM images, and corresponding height cross-sectional profiles of **A** GO1, **B** GO1–PEI, **C** GO2, and **D** GO5 networks; PFQNM mode DMT modulus (**E1**) and deformation channels of the GO5 sample (**E2**); and PFQNM mode DMT modulus (**F1**) and deformation channels (**F2**) of the GO2 sample (Reproduced with permission from reference [87]. Copyright 2023, The Authors).

materials. Graphene samples have been obtained from graphite by a microwave-assisted solvothermal technique using different low-cost solvents. The thickness layer was measured using AFM, and the number of graphene layers was assessed through AFM and XRD analysis. The thickness of the graphene layer varied between 9.87 and 587 nm, and the commercial graphene showed 2056 nm. Comparing the layer numbers obtained using the AFM technique, with those calculated using the XRD technique, it was revealed that the AFM values were higher than the XRD values. With the AFM technique, the number of layers was between 1250.298 and 6137.313, while with the XRD technique, the values varied between 2 and 25 [89].

The study of the electrical properties of graphene sheets is performed using the conductive AFM (C-AFM) method, where a probe conductive is in contact with the sample, and a bias voltage is applied generating a current flow [88, 90, 91]. Lim et al. [88] synthesized monolayer graphene flakes through CVD on copper. Figure 11A and B show AFM images of topography and the current map of a CVD-grown graphene flake. The force–distance curve obtained during their experiment exhibited a pull-off force of 57.6 ± 13 nN with a force of/under 3 nN (Fig. 11C). In Fig. 11D, the resistance profile of the CVD-grown graphene flake, plotted versus the distance from the AFM tip to the electrode, can be observed. Analyzing the fitting of the resistance curve (excluding the low-conductive spots), the authors estimated the electrical conductivity of the CVD-grown monolayer graphene flakes as $1.46 \pm 0.82 \times 10^6$ S/m [88].

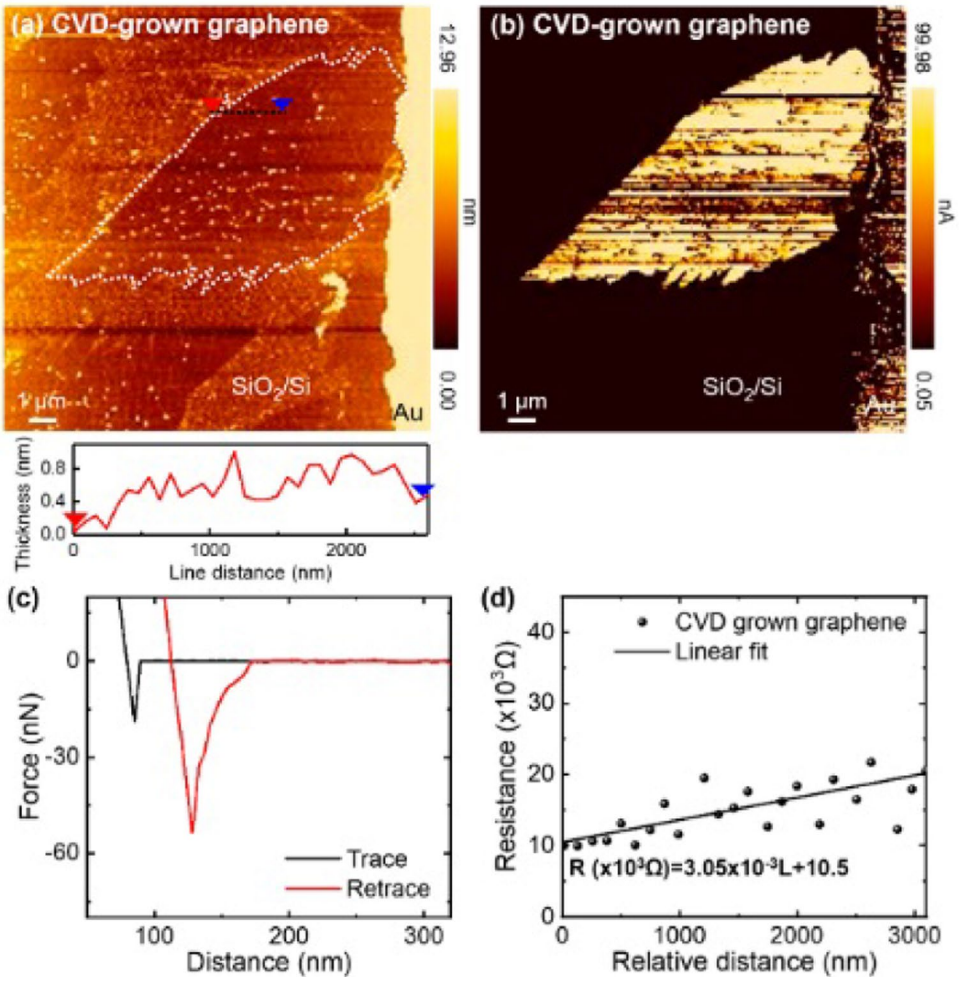


Figure 11 **A** Topography and **B** current distribution; **C** force-distance curve; and **D** resistance profile of the graphene flake (growth in SiO_2) (Reproduced with permission from reference [88]. Copyright 2021, The Authors).

Brunauer–Emmett–Teller method

The BET specific surface area and pore distribution techniques are extensively used to estimate the maximum adsorption capacity of graphene materials. In this way, the surface area and pore size distribution play significant roles in determining the materials' efficiency, capacity, and yield [7, 10].

ISO/TS 21356-1:2021 provides a method for measuring the specific surface area for dry particulates of mono-, bi- or few-layer graphene and graphitic materials, not including materials with GO or graphite oxide [16]. Before gas sorption analysis, samples must undergo degassing to eliminate any contaminants adsorbed on their surfaces. Two methods are available (i) degassing under vacuum at elevated temperatures, and (ii) degassing under inert gas flow at high temperatures. The amount of sample to be measured is contingent upon the material's surface area, typically ranging from 5 m^2 to 10 m^2 of the total surface area, with a minimum of 0.1 g of sample required.

The temperature for degassing can be selected based on the thermogravimetric analysis, opting for the highest temperature that does not induce structural or chemical changes in the sample. The duration of degassing can be established experimentally. In the end of the assay, the sample must be cooled under vacuum or inert gas until it reaches room temperature, and then must be weighed again. The typical partial pressure range used for determining BET-specific surface area is 0.05 *P*/*P0* to 0.3 *P*/*P0* but, for graphitic carbons, this range may be smaller, for example, 0.01 *P*/*P0* to 0.25 *P*/*P0*. The BET specific surface area of the samples should be calculated by applying the BET method to the sorption isotherms (Eq. 3):

$$\frac{1}{V\left[\left(\frac{P0}{P}-1\right)\right]}=\frac{1}{VmC}+C-\frac{1}{VmC}\left(\frac{P}{P0}\right) \tag{3}$$

where V is the volume of gas adsorbed at a relative pressure $P/P0$ (extracted from the isotherm), $Vm$is the volume of gas corresponding to a monolayer covering, P is the equilibrium pressure of the gas (extracted from the isotherm), P_0 is the saturation pressure (extracted from the isotherm), and C is the BET constant.

Graphene aerogel (GA) is ideal for various environmental applications, such as adsorbents, photocatalysts, and electrochemical sensors [92]. These applications are possible due to their large surface area, porous structure, low density, and thermal stability. Trinh et al. [93] synthesized GA from GO by chemical reduction using ethylenediamine (EDA) as the reducing agent with low toxicity. Briefly, after the synthesis of GO from graphite, EDA was added to the sampler and heated (90 °C), at different times, to form graphene hydrogel. Then, the graphene hydrogel was sublimated by immersion in ethanol and water (1:3) for 48 h. The best time for the reduction process of GO was selected to be 6 h. The GA produced shows a density of 4.57 mg/cm^3, a BET-specific surface area of 845 m^2/g, and a pore size of 50 μm. These results provided a maximum adsorption capacity (Langmuir model) of 149.25 mg/g of Cd^{2+} ions from water [93].

In a recent publication, an environmentally friendly method for obtaining GO using waste rice was proposed. AFM and TEM investigations unveiled that the thickness of the GO nanosheets was approximately 4 nm, with porous sizes ranging from 3 to 10 nm. The BET-specific surface area was measured at 1505 m^2/g, followed by a specific capacitance of 158.6 F/g. Based on these findings, the authors estimate the promising utility of waste rice for GO production [94].

Thermogravimetric analysis

TGA is used to study the behavior of weight loss of materials to the heat treatment. The results of TGA are shown through thermograms displaying the change in mass (mg or %) of the sample as a function of temperature or time. Another form of presentation is the first derivative thermogravimetry (DTG), which is performed by mathematical analysis, and commonly displayed as mass per minute (w/min) or percentual weight per minute (w%/min) [36].

TGA/DTG technique is a robust analytical tool to obtain qualitative and quantitative information about quality of graphene materials. It offers dependable quality control measures, enabling the classification of produced few-layer graphene materials available in the market while effectively discriminating against counterfeit or "fake graphene" samples [38]. To perform the analysis, the IEC/TS 62607-6-18:2022 is suggested (Item 3.3) [63].

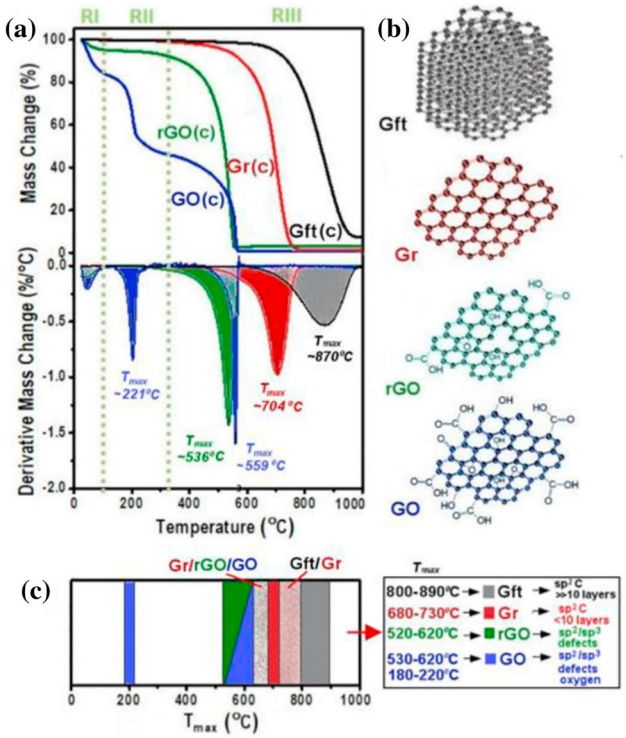


Figure 12 **a** TGA and **b** DTG graphs of graphite (Gft), graphene (Gr), rGO, and GO. **b** Representation of structures of Gft, Gr, rGO, and GO. **c** Graph presenting T_{max} ranges used for the qualitative identification of Gft, Gr, rGO, and GO (Reproduced with permission from reference [38]. Copyright 2021, Elsevier).

Figure 12 presents TGA and DTG plots of these control materials. The graphs in Fig. 12 illustrate the characteristic parameters associated with the materials, including thermal stability (the temperature at which decomposition initiates), the position and shape of the DTG peak range, and T_{max}. These parameters are closely connected to the intrinsic chemistry and physics of the materials' structures. The TGA/DTG graphs reveal the presence of three primary temperature regions, each accompanied by characteristic mass loss steps. In the first region (RI), the thermic event occurs at ~ 100 °C and is attributed to water evaporation. The thermic event corresponding to the second region (RII) occurs in the range of 100–360 °C and is attributed to the decomposition of oxygen-containing groups. The third region (RIII), in

the range of 360–1000 °C, is associated with carbon combustion [38].

Farivar et al. (2021) [38] described that graphite, characterized by a high number of stacked layers, exhibits very high DTG peaks and T_{max} values. The GO, which underwent intensive oxidation, displayed a high density of defects and nongraphitic sp^3 hybridized carbon, leading to delayed decomposition temperatures and higher T_{max} values compared with graphite. By contrast, rGO exhibited a similar DTG pattern in the RIII region compared with GO, indicating that the reduction process did not occur completely, with defective sp^3 carbon structures. However, the absence of a DTG peak in the RII region suggests that most of the oxygen functional groups were removed during the reduction process, distinguishing it from GO [38].

The incorporation of H_2O_2 into an aqueous medium during the production of graphene via the electrochemical exfoliation technique has been explored [95]. Without H_2O_2, graphene showed TGA/DTG graphs with the presence of three temperature regions followed by weight-loss stages: (I) water evaporation at ~ 100 °C, (II) the removal of oxygen functional groups above 200 °C, and the decomposition of graphene between (III) 470 and 700 °C. However, when H_2O_2 was added, graphene only exhibited a negligible mass loss of 40–60 °C, indicating the loss of adsorbed solvent molecules. Furthermore, heating the graphene above 58 °C led to significant mass loss, indicating its disintegration. The T_{max} values for graphene produced with H_2O_2 were lower than those obtained by graphene produced with the absence of H_2O_2, indicating an improved performance [95].

In-line four-point probe

The electrical conductivity is one of the most important factors in determining the application and control of graphene, depends directly on factors, such as structural quality, defects, contamination, and stiffness. The sheet resistance (R_S) provides a global measure of the local conductivity in graphene samples with infinite and finite dimensions. ISO/TR 19733: 2019 and IEC/TS 62607-6-8:2023 have standardized a method to determine R_S (Ω/sq) of graphene samples through the 4PP method [42].

The measurement range for *Rs* of the graphene samples, with the method described in this document, goes from 10^{-2} Ω/sq to 10^4 Ω/sq. No special sample preparation is required, but the substrate supporting the graphene layer should be planar and insulating. The instrumentation required for measuring monolayer CVD graphene should have a current source range of 1 μA to 1 mA and a voltmeter range of 1 mV to 1 V. However, the current applied measurement shall not damage the sample but be large enough to get accurate readings from the voltmeter. The required ambient conditions are T = 23 ± 1 °C and RH = 50 ± 4%, and the measurement should be performed with two currents equal in nominal magnitude and opposite in sign.

In 4PP method, a device equipped with four colinear probes, evenly spaced, is employed to establish electrical contact with the material. To determine the R_S, an electric current is applied, and the resistance is measured by the milli-ohmmeter. Using the information collected, the sheet resistance can be calculated using Eq. 4:

$$Rs = \frac{\pi}{\ln(2)}\frac{\Delta V}{I} = 4.53236\frac{\Delta V}{I} \tag{4}$$

where R_S is the sheet resistance (expressed in Ω/sq.), ΔV is the voltage drop measured across the inner probes, and I is the current applied at the outer probes [40, 42].

However, Eq. 3 is only valid in the ideal case of a plan surface with homogeneous resistance behavior, small thickness and the distance between the probes should be known, as well as the distance between the current probes and the edge. If this is not the case, a correction factor is required, considering the sample size, shape, thickness, and position of the probes [40, 42]. Thus, the sheet resistance can be used to calculate its resistivity (Eq. 5) and electrical conductivity (EC; Siemens—*S*) of the material, as in Eq. 6:

$$Rs = \frac{\rho}{t_f} \tag{5}$$

$$EC = \frac{1}{\rho} \tag{6}$$

where ρ is resistivity and t_f is film thickness [40].

Reduced graphene oxide thin films prepared using ultrasonic spray coating method followed by thermally annealed were evaluated for conducted

sheet-resistance measurements. For the 3× spray passes, the sheet resistance values ranged from 2 to 3.6 kΩ/sq, while for the 4× spray passes, they ranged from 1 to 3 kΩ/sq across the wafer. However, the four-point probe was able to measure only two wafers for 2 × spray passes. This limitation arose because the 2× spray passes resulted in very thin films, causing some of the GO droplets not to overlap with each other. Consequently, the wafer did not achieve full conductivity, leading to higher sheet resistance values compared to the other two spray passes. Most of the wafers subjected to 3× and 4× spray passes exhibited less than 20% sheet resistance nonuniformity [96].

L-ascorbic acid (vitamin C) has been investigated as an environmentally friendly reduction agent, of graphene oxide films. Tas et al. [97] examined the impact of L-ascorbic acid solutions, in different concentration, on the conductivity of the rGO. Based on the obtained results, the most effective reduction of GO occurred with a combination of 800 mM L-ascorbic acid and progressive thermal treatment (70, 120, and 300 °C), in which the surface resistivity was 13.2 kΩ/sq [97].

Another IEC (62607-6-1:2020, [98]) established the volume resistivity (or volume conductivity) method to determine the electrical properties of commercial graphene powders. In this method, the powder sample is pelletized using a pelletizer composed of a 4PP head, a piston, and a cylinder. To generate a uniform thickness of a sample pellet, the powder sample should be dried under vacuum, at 80 °C for 24 h, to remove any remnant of water content in the sample. The minimum thickness of the pellet is its thickness at the maximum pressure, calculated using the graphene density (assumed that the density of the graphene pellet is the same as the theoretical density of graphite, 2.3 g/cm^3), the inner diameter of the cylinder, and the sample amount. The thickness (t) can be calculated using Eq. 7.

$$t = \frac{m}{d_{gr}A} \tag{7}$$

where t is the specimen (pellet) thickness measures by thickness gauge equipped in the apparatus, d_{gr} is the theoretical density of graphite (2.3 g/cm^3), m is the amount of the sample, and $A$is the cross-sectional area of the piston.

After determining the amount of the powder graphene, the sample is accommodated inside the cylinder and pressured at pressure from 2.6 MPa to 52 MPa, with a 2.5 MPA interval. The resistance values are recorded via the 4PP system, and the volume resistivity is calculated considering the pellet thickness, measured simultaneously with sheet resistance, and geometric dimensions. The volume resistivity (ρv) of a pellet is calculated using Eq. 8 and volume conductivity using Eq. 9.

$$\rho v = R.F.t \tag{8}$$

where ρv is the volume resistivity, R is the resistance measured by 4PP measurement system ($R = V/I$), t is the specimen (pellet) thickness measured by thickness gauge equipped in the apparatus, and F is the geometrical correction factor.

$$\sigma V = \frac{1}{\rho v} \tag{9}$$

where σV is the volume conductivity; and ρv is the volume resistivity.

Resonant cavity

The microwave resonant cavity method is appealing for measuring surface conductance (σ_G), because it is non-destructive and experimentally simple, making it suitable for research and development, and for quality control in the manufacturing of graphene materials, including nano-size structures [43].

IEC TS 62607-6-4:2024 established the surface conductance measurement by the resonant cavity of graphene materials synthesized by CVD on metal substrates, epitaxial growth on silicon carbide, obtained from rGO, or mechanically exfoliated from graphite [44]. The typical surface conductance value of graphene materials can be between 1 S (for few-layer graphene and/or doped graphene) and 10^{-5} S (for single graphene layer). The thickness of the sample does not need to be known, but a lateral dimension should be considered, and the substrate may be non-conducting substrate (fused silica wafer or silicon carbide without Si- or C- terminated face).

Recently, IEC TS 62607-6-4:2024 was published as a technical revision of IEC TS 62607-6-4:2016 [45]. The new edition includes technical changes concerning the previous edition such as: (i) changing the document title and (ii) replacing figures, to better illustrate the fundamentals of the method and its implementation for a non-technical reader.

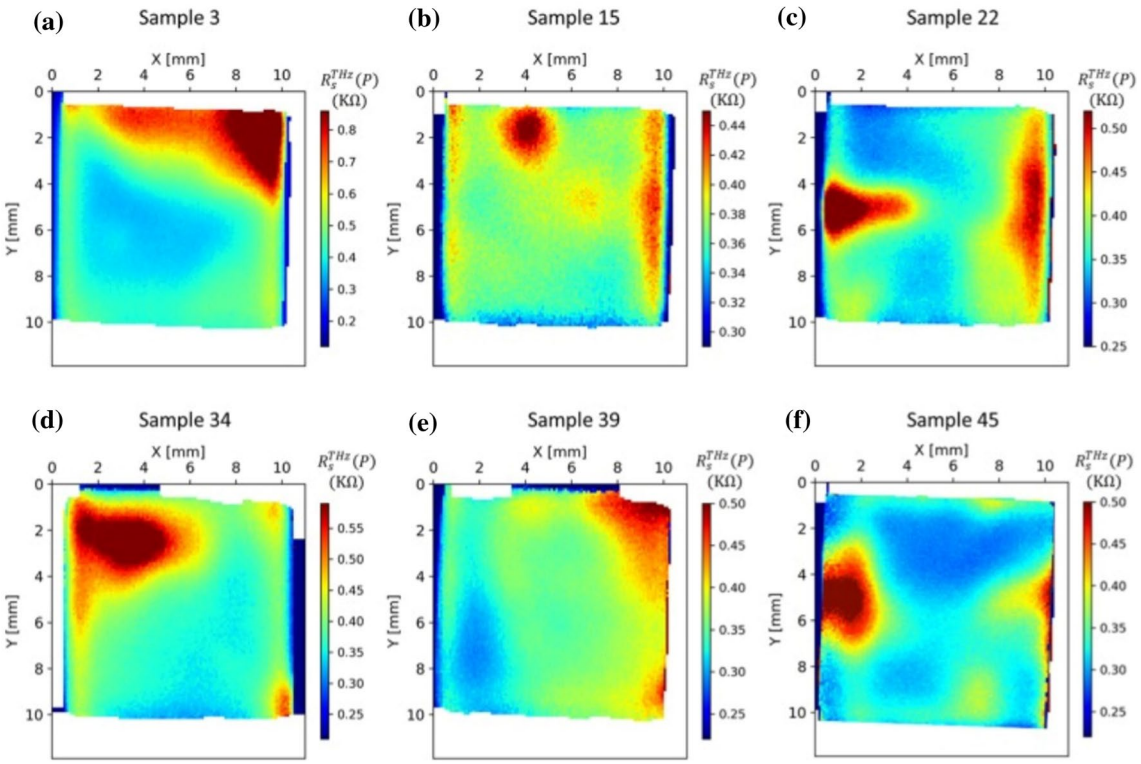


Figure 13 Representative sheet resistance maps (Reproduced with permission from reference [99]. Copyright 2020, The Authors).

For a better understanding, a guide with the good practice on the electrical characterization of graphene using resonant cavity method was created by Grace Consortium group [46]. In this guide, the researcher can find the details of the resonant cavity method, according to IEC TS 62607-6-4:2016 [45]. Moreover, the study developed by Obrzut et al. [43] described in detail the microwave resonant cavity method on the surface conductance of graphene of epitaxial monolayer graphene on SiC and CVD graphene.

Terahertz time-domain spectroscopy

THz-TDS is a measurement technique that enables a noncontact and nondestructive assessment of the electrical properties of graphene. This versatile method allows for the spatial mapping of key parameters, such as DC conductivity (σDC), scattering time (τ), carrier density (n), and mobility (μ) on different substrates commonly used with graphene (Si, quartz, SiC, sapphire, and polymers). Briefly, an electromagnetic short pulse is directed at the material composed of graphene (reflected or transmitted), where the resulting THz signal is in an electric field form, and when subjected to

Table 3 Values conductance/resistance measured (M ± SD) from THz maps rGO (Reproduced with permission from reference [99]. Copyright 2020, The Authors)

Sample	Average (mS)/(kΩ/sq)	Standard deviation (mS)/(kΩ/sq)	Variation coefficient (%)
S3	2.16/0.46	0.52/0.110	24
S15	2.64/0.38	0.13/0.019	5
S22	2.65/0.37	0.30/0.041	11
S34	2.43/0.41	0.37/0.062	15
S39	2.82/0.35	0.23/0.028	8
S45	2.69/0.37	0.33/0.052	14

Fourier transformation gives rise to both amplitude and phase information in a wide THz spectral range [47–49]. IEC/TS 62607-6-10:2021 established a standardized method for determining the sheet resistance (R_S) for films of graphene-based materials through THz-TDS [49]. It allows for two measurement configurations, i.e., transmission and reflection. Although either setup is sufficient for obtaining resistance values, the employment of both may reduce measurement errors. The measurements should be performed

Table 4 Technique recommendations according to ISO/IEC for graphene characterization

Technique	Applications	Parameters	Limitations	ISO/IEC
UV–vis	Investigates the degree of graphene oxidation Sample preparation	Dispersion in deionized water; Sonication by 10 min, 120 W and 40 Hz	Dispersion in deionized water	ISO/TS 21356-1: 2021
Raman spectroscopy	Determination of the defect level	Sample should form a tablet on a flat substrate; Wavelength: 514 nm, 532 nm, and 633 nm	Applied for powders graphene-based materials	IEC/TS 62607-6-14: 2020
	Determination of the strain uniformity	Sample bigger than the Raman laser spot size; Insulating substrate or copper substrate; Laser power lower than 1 mW Spot size below 1 µm; Spectral resolution > 1,5 cm^{-1}; For maps, a square area of 10 µm × 10 µm	Applied for single-layer graphene	IEC/TS 62607-6-6: 2020
FTIR	Identify functional groups	ATR measurement; In association with TGA analysis the suggested parameters are: Spectrum scope: 400 cm^{-1}–4000 cm^{-1} Resolution factor: 8 cm^{-1}	–	IEC/TS 62607–6-18: 2022
XPS	Determination of the elemental composition and C/O ratio	Sample in pellet form; Vacuum pressure lower than 5×10^{-8} mbar; Energy range: 0–1000 eV; CPS value at C 1s peak should be $\geq 1 \times 10^{5}$	Applied for powders graphene-based materials	IEC/TS 62607–6-21: 2022
XRD	Determine the typical order parameters; Differentiating few-layer graphene or rGO from layered carbon material	Preparation method of sample: An amount of sample should be deposited in groove loader and pressed with glass slide, covering the center of the groove	Applied for powders graphene-based materials Not applied for GO samples	IEC/TS 62607–6-17: 2023

Table 4 continued

Technique	Applications	Parameters	Limitations	ISO/IEC
SEM	Evaluate sample surface and lateral size	Preparation method of sample: Dispersion in deionized water or isopropanol; Sonication by 10 min, 120 W and 40 Hz Use 100–100 0 μL onto support grid (silicon dioxide substrate); Gold powder can be used to cove the sample Acceleration voltage < 5KN; Use more than 200 flakes for analysis	Applied for graphene flakes samples	ISO/TS 21356-1: 2021
TEM	Determine the typical order parameters	Preparation method of sample: Dispersion in absolute ethanol; Sonication by 15 min, 120 W and 40 Hz Use 2 μL onto TEM grid; Dry naturally for 1 h before analysis	–	IEC/TS 62607-6-17:2023
	Determine the lateral size, number of layers, and alignment between layers of sample	Preparation method of sample: Dispersion in solvent; Shaking until complete dispersion; Use 100–200 μL onto TEM grid; ry at ~ 150 °C under vacuum for 8 h Resolution ≥ 0.2 nm Accelerating voltage ≤ 80 kV	Applied for graphene flakes samples with lateral size < 3 μm	ISO/TS 21356-1: 2021

Table 4 continued

Technique	Applications	Parameters	Limitations	ISO/IEC
AFM	Determine the lateral size and thickness	Preparation method of sample: Dispersion in deionized water or isopropanol; Sonication by 10 min, 120 W and 40 Hz Use 100–100 0 µL onto support grid Probe with intermittent contact: Spring constant: ~ 40 N/m; Resonance frequency: 240 kHz; Apex size: 5- 15 nm; Scan area (1): 20 µm × 20 µm, scan speed:10 µm/s, resolution 256 pixels × 256 pixels; Scan area (2): 2 µm × 2 µm, resolution 512 pixels × 512 pixels;	Applied for graphene flakes	ISO/TS 21356–1: 2021
BET	Determine the maximum adsorption capacity of sample	Sample should be degassing by vacuum or inert gas at elevated temperatures; Total surface area of sample: 5 – 10 m^2 (mass sample > 0.1g) Temperature can be determined by thermogravimetric analysis; Time can be determined experimentally; Typical partial pressure range is 0.05 *P/P0* to 0.3 *P/P0*	Not applied for GO or graphite oxide samples	ISO/TS 21356-1: 2021
TGA	Demonstrate the behavior of weight loss of sample	Mass sample: ≥ 5 mg; Temperature: 25 – 1,200 °C Heating rate: 5 °C/min Flow rate: 50 mL/min	–	IEC/TS 62607-6-18: 2022
4PP	Determine the sheet resistance of sample	No special sample preparation; Substrate supporting planar and insulating/quartz; Source: 1 µA – 1 mA; Voltmeter: 1 mV – 1 V; Temperature: 23 °C ± 1 °C; Relative humidity: 50 ± 4%; Distance between probes known	Applied for CVD graphene	IEC/TS 62607–6-8:2023

Table 4 continued

Technique	Applications	Parameters	Limitations	ISO/IEC
Resonant cavity	Determine surface conductance	Substrate: silica wafer (200 um to 250 um thick); Automatic two-port vector network analyzer operating in the frequency range that covers the frequency band (6,6 GHz to 13 GHz); Dynamic range of the measurements: ≥ 70 dB; IEEE 488 I/O interface or equivalent	Applied for CVD graphene	IEC TS 62607-6-4:2024
THz-TDS	Determine the sheet resistance of sample	Two modes: transmission and reflection; Parameters prescribed by equipment or: Temperature: 10–37 °C; Relative humidity: 70%; Atmosphere: air, nitrogen or argon; Pressure: atmospheric or under vacuum	Applied for graphene films	IEC/TS 62607-6-10:2021

to the prescribed parameters for THz spectroscopy equipment or conducted within a temperature range of 10 °C < T < 37 °C, with relative humidity below 70%, and within an atmosphere of air, nitrogen, or argon at atmospheric pressure or under vacuum [49]. Figure 13 shows an example of sheet resistance maps obtained from the THz-TDS system, indicating areas of inhomogeneous sheet resistance.

Table 3 summarizes the conductance and resistance values (M ± SD) obtained from the THz maps. The sheet resistance maps show features as spots or islands with higher sheet resistance, in special for 15, 22, 34, and 45 samples., while samples 3 and 39 showed two distinct sheet resistance areas. These features can be related to the presence of microscopic defects, such as cracks, and the presence of growth domains [99].

Alternative method to determine the graphene domain

The electrical, thermal, and mechanical properties of graphene with 2D structure are related to the size and distribution of graphene domains and defects (pinholes, domain boundaries, and cracks). As graphene domain size is increased and graphene defects are reduced, the graphene electrical and thermal properties are improved [100, 101].

Determination of the domain size is addressed in IEC/TS 62607-6-3:2020 [102]. This guideline established a fast, easy and reliable standardized method to evaluate CVD graphene domains formed on copper by oxidation. To apply this method, described in this guideline, the test sample should be removed from the production process and put in an oxidation chamber with humidity control (25–80%) and a Hg lamp (20 mW/cm^2–70 mW/cm^2) for 5 min and no more than 60 min. If a hot plate is used to accelerate oxidation, the temperature of the hot plate is between 100 °C and 200 °C. The oxidation procedure does not change the domain size. A conventional optical microscope (or a scanning electron microscope) is used to measure. An image analysis program, such as Image J, can be used for measuring the size of the graphene domains where the number of pixels in the domain will be counted first and converted into the size of the domain in the area (cm^2 or μm^2) by multiplying the number of pixels in the domain by the size of pixels [102].

Conclusions

An overview of the essential techniques for characterizing graphene, following the ISO/IEC standards, has been provided in this review and are summarized in Table 4. The guidelines have some limitations, such as the types of samples covered in the different methods. Scientists have used various techniques to study the structure, mechanical properties, number of layers, conductivity, and morphology of nanomaterials based on graphene. These studies described in the literature by independent authors do not always follow standardized techniques (ISO/IEC), allowing to characterize different graphene samples using different methods. In this way, comparing results from other research groups is a laborious task. Most scientific articles only report successful cases of characterization techniques and fail to present and discuss the observed phenomena during synthesis and characterization. Researchers and industry professionals would use these standard techniques to ensure quality, improve of performance, validate synthesis methods, and identify "fake graphene."

Acknowledgements

This research was funded by the National Council for Scientific and Technological Development (CNPq/MCTI/FNDCT, Brazil), grant number 408377/2022-4. It was conducted within the framework of the National Institute of Science and Technology in Pharmaceutical Nanotechnology: A Transdisciplinary Approach (INCT-NANOFARMA, which is supported by the São Paulo Research Foundation (FAPESP, Brazil) Grant #2014/50928-2, and also by the National Council for Scientific and Technological Development (CNPq, Brazil) Grant #465687/2014-8. Eliana B. Souto acknowledges the national funds from FCT—Fundação para a Ciência e a Tecnologia, I.P., Lisbon, Portugal.

Author contributions

Conceptualization: T.A., M.C., and P.S.; methodology: T.A. and M.C.; investigation: T.A., W.S.M., D.A., and D.K.; writing—original draft preparation: T.A., C.B., M.C., and J.C.C.; writing—review and editing: T.A., E.B.S., and A.Z.; and visualization version: T.A., M.C. and P.S.; project administration, supervision and funding: E.B.S. and M.C. All authors have read and agreed to the published version of the manuscript.

Funding

Open access funding provided by FCT|FCCN (b-on).

Data availability

No data were created in this review.

Declarations

Conflict of interest The authors declare that there are no conflicts of interest.

Ethical approval This review does not raise any ethics issues.

Open Access This article is licensed under a Creative Commons Attribution 4.0 International License, which permits use, sharing, adaptation, distribution and reproduction in any medium or format, as long as you give appropriate credit to the original author(s) and the source, provide a link to the Creative Commons licence, and indicate if changes were made. The images or other third party material in this article are included in the article's Creative Commons licence, unless indicated otherwise in a credit line to the material. If material is not included in the article's Creative Commons licence and your intended use is not permitted by statutory regulation or exceeds the permitted use, you will need to obtain permission directly from the copyright holder. To view a copy of this licence, visit http://creativecommons.org/licenses/by/4.0/.

References

[1] Mbayachi VB, Ndayiragije E, Sammani T, Taj S, Mbuta ER, Khan, AU (2021) Graphene synthesis, characterization and its applications: a review. Results Chem 3:100163

[2] Shu R, Nie L, Zhao Z, Yang X (2024) Synthesis of nitrogen-doped reduced graphene oxide/magnesium ferrite/polyaniline composite aerogel as a lightweight, broadband and efficient microwave absorber. J Mater Sci Technol 175:115–124

[3] Chang L, Wang Y-Z, Zhang X-C, Li L, Zhai H-Z, Cao M-S (2024) Toward high performance microwave absorber by implanting La0. 8CoO3 nanoparticles on rGO. J Mater Sci Technol 174:176–187
[4] Cao K, Fang Y, Wang S, Zhang Y, Wen J, Chen J, Zhao R, Xue W (2024) Magnetic NiFe2O4@ FeNi3 core-shell nanospheres derived from FeNi-LDH precursor anchoring on rGO nanosheets for enhanced electromagnetic wave absorption. J Mater Sci 171:101–114
[5] Gajewska K, Moyseowicz A, Minta D, Gryglewicz G (2023) Effect of electrolyte and carbon material on the electrochemical performance of high-voltage aqueous symmetric supercapacitors. J Mater Sci 58:1721–1738
[6] Yusaf T, Mahamude ASF, Farhana K, Harun WSW, Kadirgama K, Ramasamy D, Kamarulzaman MK, Subramonian S, Hall S, Dhahad HA (2022) A comprehensive review on graphene nanoparticles: Preparation, properties, and applications. Sustainability 14:12336
[7] Abbas Q, Shinde PA, Abdelkareem MA, Alami AH, Mirzaeian M, Yadav A, Olabi AG (2022) Graphene synthesis techniques and environmental applications. Materials 15:7804
[8] Ibrahim A, Klopocinska A, Horvat K, Abdel Hamid Z (2021) Graphene-based nanocomposites: synthesis, mechanical properties, and characterizations. Polymers (Basel) 13:2869
[9] Gutiérrez-Cruz A, Ruiz-Hernández AR, Vega-Clemente JF, Luna-Gazcón DG, Campos-Delgado J (2022) A review of top-down and bottom-up synthesis methods for the production of graphene, graphene oxide and reduced graphene oxide. J Mater Sci 57:14543–14578
[10] Fraga TJM, da Motta Sobrinho MA, Carvalho MN, Ghislandi MG (2020) State of the art: synthesis and characterization of functionalized graphene nanomaterials. Nano Express 1:022002
[11] Edward K, Mamun K, Narayan S, Assaf M, Rohindra D, Rathnayake U (2023) State-of-the-art graphene synthesis methods and environmental concerns. Appl Environ Soil Sci 1:8475504
[12] IEC, International Electrotechnical Commission, Nanomanufacturing (2022) Key control characteristics—Part 6–11: graphene—defect density: Raman spectroscopy. https://webstore.iec.ch/publication/33187. Accessed 31 Aug 2023
[13] ISO, ISO/TS 80004-13:2017 (2017) Nanotechnologies—vocabulary—Part 13: Graphene and related two-dimensional (2D) materials. Accessed 31 Aug 2023
[14] ISO, ISO/TS 80004-3:2020 (2020) Nanotechnologies—vocabulary—Part 3: Carbon nano-objects. https://www.iso.org/standard/75335.html. Accessed 31 Aug 2023
[15] ISO, ISO/TR 19733:2019 (2019) Nanotechnologies—matrix of properties and measurement techniques for graphene and related two-dimensional (2D) materials. https://www.iso.org/standard/66188.html. Accessed 1 Sep 2023
[16] ISO, ISO/TS 21356-1:2021 (2021) Nanotechnologies—structural characterization of grapheme—Part 1: graphene from powders and dispersions. https://www.iso.org/standard/70757.html. Accessed 1 Sep 2023
[17] Seekaew Y, Arayawut O, Timsorn K, Wongchoosuk C, Chapter Nine—Synthesis, characterization, and applications of graphene and derivatives, In: Yaragalla S, Mishra R, Thomas S, Kalarikkal N, Maria HJ (eds) Carbon-based nanofillers and their rubber nanocomposites. Elsevier, Amsterdam, pp 259–283
[18] Zhang Z, Schniepp HC, Adamson DH (2019) Characterization of graphene oxide: variations in reported approaches. Carbon 154:510–521
[19] Abdolkarimi-Mahabadi M, Bayat A, Mohammadi A (2021) Use of UV-Vis spectrophotometry for characterization of carbon nanostructures: a review. Theoret Exp Chem 57:191–198
[20] Orlando A, Franceschini F, Muscas C, Pidkova S, Bartoli M, Rovere M, Tagliaferro A (2021) A comprehensive review on Raman spectroscopy applications. Chemosensors 9:262
[21] Parvin N, Kumar V, Joo SW, Park S-S, Mandal TK (2022) Recent advances in the characterized identification of mono-to-multi-layer graphene and its biomedical applications: a review. Electronics 11:3345
[22] Kumar V, Kumar A, Lee DJ, Park SS (2021) Estimation of number of graphene layers using different methods: a focused review. Materials (Basel) 14:4590
[23] Li Z, Deng L, Kinloch IA, Young RJ (2023) Raman spectroscopy of carbon materials and their composites: graphene, nanotubes and fibres. Prog Mater Sci 135:101089
[24] NNovais GB, Dias MA, Santana AAM, Batista TC, Marques MN, Melo CR, Albuquerque RLC, Gomes MZ, Severino P, Souto EB, Cardoso JC (2023) Isoflavones-functionalized single-walled and multi-walled carbon nanotubes: synthesis and characterization of new nanoarchitetonics for biomedical uses. J Mol Struct 1294:136351
[25] Samal RR, Gautam D, Panmei K, Lanbiliu P, Saya L, Gambhir G, Hooda S, Kumar S (2022) Evolution in graphene oxide-based materials characterization and modeling. In: Reference module in materials science and materials engineering, Elsevier
[26] Krishna DNG, Philip J (2022) Review on surface-characterization applications of X-ray photoelectron spectroscopy (XPS): recent developments and challenges. Appl Surf Sci Adv 12:100332
[27] Firas Habeb A, Ayad Fadel A, Falah Hasan H (2019) Behavior of X-ray analysis of carbon nanotubes. In: Hosam El-Din S, Said Moawad Mohamed ES (eds) Perspective of carbon nanotubes, IntechOpen, Rijeka, p 7
[28] Gascho JLS, Costa SF, Recco AAC, Pezzin SH (2019) Graphene oxide films obtained by vacuum filtration: X-ray diffraction evidence of crystalline reorganization. J Nanomater 2019:5963148
[29] Jeon I (2018) Graphene at interfaces; PhD Thesis, Department of Materials Science and Engineering, Massachusetts Institute of Technology, https://dspace.mit.edu/bitstream/handle/1721.1/117790/1051211579-MIT.pdf?sequence=1. Accessed 1 Jul 2024
[30] Aarva A, Sainio S, Deringer VL, Caro MA, Laurila T (2021) X-ray spectroscopy fingerprints of pristine and functionalized graphene. J Phys Chem C 125:18234–18246
[31] Ganya ES, Soin N, Moloi SJ, McLaughlin JA, Pong WF, Ray SC (2020) Polyacrylate grafted graphene oxide nanocomposites for biomedical applications. J Appl Phys 127:054302
[32] Meyer JC (2021) Transmission electron microscopy characterization of grapheme. In: Skakalova V, Kaiser AB (eds), Graphene, 2nd edn, Ch 13. Woodhead Publishing, Cambridge, pp 317–343
[33] Teklu A, Barry C, Palumbo M, Weiwadel C, Kuthirummal N, Flagg J (2019) Mechanical characterization of reduced graphene oxide using AFM. Adv Condensed Matter Phys 2019:8713965
[34] De Silva KKH, Huang H-H, Viswanath P, Joshi R, Yoshimura M (2022) Nanoscale electrical characterization of graphene-based materials by atomic force microscopy. J Mater Res 37:3319–3339
[35] Nguyen-Tri P, Ghassemi P, Carriere P, Nanda S, Assadi AA, Nguyen DD (2020) Recent applications of advanced atomic force microscopy in polymer science: a review. Polymers (Basel) 12:1142

[36] Du W, Ma R, Liu Z, Yang G, Chen T (2021) Study on the adsorption properties of graphene oxide/laponite RD/chitosan composites. Materials (Basel) 14:3224
[37] Mohan VB, Jayaraman K, Bhattacharyya D (2020) Brunauer–Emmett–Teller (BET) specific surface area analysis of different graphene materials: a comparison to their structural regularity and electrical properties. Solid State Commun 320:114004
[38] Farivar F, Yap PL, Hassan K, Tung TT, Tran DNH, Pollard AJ, Losic D (2021) Unlocking thermogravimetric analysis (TGA) in the fight against "Fake graphene" materials. Carbon 179:505–513
[39] Farivar F, Lay Yap P, Karunagaran RU, Losic D (2021) Thermogravimetric analysis (TGA) of graphene materials: effect of particle size of graphene, graphene oxide and graphite on thermal parameters. J Carbon Res 7:41
[40] Naftaly M, Das S, Gallop J, Pan K, Alkhalil F, Kariyapperuma D, Constant S, Ramsdale C, Hao L (2021) Sheet resistance measurements of conductive thin films: a comparison of techniques. Electronics 10:960
[41] Cultrera A, Serazio D, Zurutuza A, Centeno A, Txoperena O, Etayo D, Cordon A, Redo-Sanchez A, Arnedo I, Ortolano M, Callegaro L (2019) Mapping the conductivity of graphene with electrical resistance tomography. Sci Rep 9:10655
[42] IEC, TS 62607-6-8:2023 (2023) Nanomanufacturing—key control characteristics—Part 6–8: graphene-sheet resistance: in-line four-point probe. https://webstore.iec.ch/publication/32302. Accessed 27 Dec 2023
[43] Obrzut J, Emiroglu C, Kirillov O, Yang Y, Elmquist RE (2016) Surface conductance of graphene from non-contact resonant cavity. Measurement 87:146–151
[44] IEC, TS 62607-6-4:2024 (2024) Nanomanufacturing—key control characteristics—Part 6–4: graphene-based materials—surface conductance: non-contact microwave resonant cavity method. https://www.csagroup.org/store/product/iec_068258/. Accessed 1 Jul 2024
[45] IEC, TS 62607-6-4:2016 (2016) Nanomanufacturing—key control characteristics—Part 6–4: grapheme—surface conductance measurement using resonant cavity, chrome-extension://efaidnbmnnnibpcajpcglclefindmkaj. https://webstore.iec.ch/p-preview/info_iects62607-6-4%7Bed1.0%7Den.pdf. Accessed 1 Jul 2024
[46] 16NRM01, EMPIR GRACE Consortium (2020) In: Fabricius A, Cultrera A, Catanzaro A (eds), Good practice guide on the electrical characterisation of graphene using noncontact and high throughput methods, ISBN: 978-88-945324-2–5. http://empir.npl.co.uk/grace/. Accessed 1 Jul 2024
[47] Mølvig BH, Bæk T, Ji J, Bøggild P, Lange SJ, Jepsen PU (2023) Terahertz cross-correlation spectroscopy and imaging of large-area graphene. Sensors 23:3297
[48] Whelan PR, Zhou B, Bezencenet O, Shivayogimath A, Mishra N, Shen Q, Jessen BS, Pasternak I, Mackenzie DMA, Ji J, Sun C, Seneor P, Dlubak B, Luo B, Østerberg FW, Huang D, Shi H, Luo D, Wang M, Ruoff RS, Conran BR, McAleese C, Huyghebaert C, Brems S, Booth TJ, Napal I, Strupinski W, Petersen DH, Forti S, Coletti C, Jouvray A, Teo KBK, Centeno A, Zurutuza A, Legagneux P, Jepsen PU, Bøggild P (2021) Case studies of electrical characterisation of graphene by terahertz time-domain spectroscopy. 2D Materials 8:022003
[49] IEC, TS 62607-6-10:2021 (2021) Nanomanufacturing—key control characteristics—Part 6–10: graphene-based material-sheet resistance: terahertz time-domain spectroscopy. https://webstore.iec.ch/publication/28888. Accessed 27 Dec 2023
[50] Cayambe M, Zambrano C, Tene T, Guevara M, Tubon Usca G, Brito H, Molina R, Coello-Fiallos D, Caputi LS, Vacacela Gomez C (2021) Dispersion of graphene in ethanol by sonication. Mater Today Proc 37:4027–4030
[51] Ojrzynska M, Wroblewska A, Judek J, Malolepszy A, Duzynska A, Zdrojek M (2020) Study of optical properties of graphene flakes and its derivatives in aqueous solutions. Opt Express 28:7274–7281
[52] Sherif HHA, El Hotaby W, Khalil SKH, Hemdan BA, Khalil WA (2023) Preparation, characterization, and biological assessment of functionalized reduced graphene oxide–silver nanocomposite. J Mater Res 38:1843–1857
[53] Tene T, Tubon Usca G, Guevara M, Molina R, Veltri F, Arias M, Caputi LS, Vacacela Gomez C (2020) Toward large-scale production of oxidized graphene. Nanomater (Basel, Switz) 10:2–279
[54] IEC, IEC/TS 62607-6-14:2020 (2020) Nanomanufacturing—key control characteristics—Part 6–14: graphene-based material—defect level: Raman spectroscopy. https://webstore.iec.ch/publication/32976. Accessed 15 Sep 2023
[55] Cançado LG, Jorio A, Ferreira EHM, Stavale F, Achete CA, Capaz RB, Moutinho MVO, Lombardo A, Kulmala TS, Ferrari AC (2011) Quantifying defects in graphene via raman spectroscopy at different excitation energies. Nano Lett 11:3190–3196
[56] Hu K, Brambilla L, Sartori P, Moscheni C, Perrotta C, Zema L, Bertarelli C, Castiglioni C (2023) Development of tailored graphene nanoparticles: preparation, sorting and structure assessment by complementary techniques. Molecules 28:565
[57] Zhang Z, Jin H, Wu C, Ji J (2018) Efficient production of high-quality few-layer graphene using a simple hydrodynamic-assisted exfoliation method. Nanoscale Res Lett 13:416
[58] Childres I, Qi Y, Sadi MA, Ribeiro JF, Cao H, Chen YP (2022) Combined raman spectroscopy and magneto-transport measurements in disordered graphene: correlating Raman D band and weak localization features. Coatings 12:1137
[59] Hwangbo Y, Lee C-K, Mag-Isa AE, Jang J-W, Lee H-J, Lee S-B, Kim S-S, Kim J-H (2014) Interlayer non-coupled optical properties for determining the number of layers in arbitrarily stacked multilayer graphenes. Carbon 77:454–461
[60] Al-Quraishi KK, He Q, Kauppila W, Wang M, Yang Y (2020) Mechanical testing of two-dimensional materials: a brief review. Int J Smart Nano Mater 11:207–246
[61] IEC, IEC/TS 62607-6-6: 2021 (2021) Nanomanufacturing—key control characteristics—Part 6–6: graphene—strain uniformity: Raman spectroscopy. https://webstore.iec.ch/publication/34162. Accessed 15 Sep 2023
[62] Pastore Carbone MG, Tsoukleri G, Manikas AC, Makarona E, Tsamis C, Galiotis C (2019) Production and mechanical characterization of graphene micro-ribbons. J Compos Sci 3:42
[63] IEC, IEC/TS 62607-6-18: 2022 (2022) Nanomanufacturing—key control characteristics—Part 6–18: graphene-based material—functional groups: TGA-FTIR. https://webstore.iec.ch/publication/62180. Accessed 20 Sep 2023
[64] Wijaya R, Andersan G, Permatasari Santoso S, Irawaty W (2020) Green reduction of graphene oxide using kaffir lime peel extract (citrus hystrix) and its application as adsorbent for methylene blue. Sci Rep 10:667
[65] Eivazzadeh-Keihan R, Alimirzaloo F, Aghamirza Moghim Aliabadi H, Bahojb Noruzi E, Akbarzadeh AR, Maleki A, Madanchi H, Mahdavi M (2022) Functionalized graphene oxide nanosheets with folic acid and silk fibroin as a novel nanobiocomposite for biomedical applications. Sci Rep 12:6205
[66] Kumar N, Srivastava VC (2018) Simple synthesis of large graphene oxide sheets via electrochemical method coupled with oxidation process. ACS Omega 3:10233–10242

[67] IEC, IEC/TS 62607-6-21: 2022 (2022) Nanomanufacturing—key control characteristics—Part 6–21: graphene-based material—elemental composition, C/O ratio: X-ray photoelectron spectroscopy. https://webstore.iec.ch/publication/62184. Accessed 22 Sep 2023
[68] Kovtun A, Jones D, Dell'Elce S, Treossi E, Liscio A, Palermo V (2019) Accurate chemical analysis of oxygenated graphene-based materials using X-ray photoelectron spectroscopy. Carbon 143:268–275
[69] Foschi M, Capasso P, Maggi MA, Ruggieri F, Fioravanti G (2021) Experimental design and response surface methodology applied to graphene oxide reduction for adsorption of triazine herbicides. ACS Omega 6:16943–16954
[70] IEC, IEC/TS 62607-6-17: 2023 (2023) Nanomanufacturing—key control characteristics—Part 6–17: grapheme—based material—order parameter: X-ray diffraction and transmission electron microscopy. https://products.iec.ch/view/pub/62179?q=eyJtb2RlIjoiUFVCTElDQVRJT04iLCJzb3J0QnkiOiJyZWZlcmVuY2UtLWFzYyIsImxhbmd1YWdlIjoiZW4ifQ%3D%3D. Accessed 2 Oct 2023
[71] Arbuzov AA, Muradyan VE, Tarasov BP (2013) Synthesis of graphene-like materials by graphite oxide reduction. Russ Chem Bull 62:1962–1966
[72] Emiru TF, Ayele DW (2017) Controlled synthesis, characterization and reduction of graphene oxide: a convenient method for large scale production. Egypt J Basic Appl Sci 4:74–79
[73] Iglesias-Juez A, Chiarello GL, Patience GS, Guerrero-Pérez MO (2022) Experimental methods in chemical engineering: X-ray absorption spectroscopy—XAS, XANES, EXAFS. Can J Chem Eng 100:3–22
[74] Sharma A, Varshney M, Nanda SS, Shin HJ, Kim N, Yi DK, Chae K-H, Ok Won S (2018) Structural, electronic structure and antibacterial properties of graphene-oxide nano-sheets. Chem Phys Lett 698:85–92
[75] Sharma A, Nanda SS, Parkash J, Sahai A, Kumar S, Maikhuri D, Yi DK, Shin H-J, Chae K-H, Won SO (2019) Structural and electronic structure investigations on sonication based synthesized graphene oxide and reduced-graphene oxide nano-sheets. Phys Scr 94:125807
[76] Sieradzka M, Ślusarczyk C, Biniaś W, Fryczkowski R (2021) The role of the oxidation and reduction parameters on the properties of the reduced graphene oxide. Coatings 11:166
[77] Ding J, Zhao H, Yu H (2021) Graphene nanofluids based on one-step exfoliation and edge-functionalization. Carbon 171:29–35
[78] Cho JH, Na SR, Park S, Akinwande D, Liechti KM, Cullinan MA (2019) Controlling the number of layers in graphene using the growth pressure. Nanotechnology 30:235602
[79] Chuah R, Gopinath SCB, Anbu P, Salimi MN, Yaakub ARW, Lakshmipriya T (2020) Synthesis and characterization of reduced graphene oxide using the aqueous extract of *Eclipta prostrata*. 3 Biotech 10:364
[80] Navik R, Gai Y, Wang W, Zhao Y (2018) Curcumin-assisted ultrasound exfoliation of graphite to graphene in ethanol. Ultrason Sonochem 48:96–102
[81] Ishida N (2024) Atomic force microscopy. In: Otsuki A, Jose S, Mohan M, Thomas S (eds) Non-destructive material characterization methods. Ch 4. Elsevier, Amsterdam, pp 89–125
[82] Garg M, Thakur A (2023) A review: biomedical applications of phosphorene, antimonene, and germanene-based 2D material/hydrogel complexes. J Mater Sci 58:34–45
[83] Xiao B, Yin M, Li W, Liang L, Dai S, Zhang X, Wang W, Liu Z (2023) Significant enhanced mechanical properties of suspended graphene film by stacking multilayer CVD graphene films. Micromachines. https://doi.org/10.3390/mi14040745
[84] Kwaśniewska A, Świetlicki M, Prószyński A, Gładyszewski G (2021) The quantitative nanomechanical mapping of starch/kaolin film surfaces by peak force AFM. Polymers (Basel) 13:244
[85] Morsink M, Severino P, Luna-Ceron E, Hussain MA, Sobahi N, Shin SR (2022) Effects of electrically conductive nano-biomaterials on regulating cardiomyocyte behavior for cardiac repair and regeneration. Acta Biomater 139:141–156
[86] Lee M, Kim MC, Lee JY (2022) Nanomaterial-based electrically conductive hydrogels for cardiac tissue repair. Int J Nanomed 17:6181–6200
[87] Pilato S, Moffa S, Siani G, Diomede F, Trubiani O, Pizzicannella J, Capista D, Passacantando M, Samorì P, Fontana A (2023) 3D Graphene oxide-polyethylenimine scaffolds for cardiac tissue engineering. ACS Appl Mater Interfaces 15:14077–14088
[88] Lim S, Park H, Yamamoto G, Lee C, Suk JW (2021) Measurements of the electrical conductivity of monolayer graphene flakes using conductive atomic force microscopy. Nanomater (Basel) 11:2575–2586
[89] Gürünlü B, Taşdelen-Yücedağ Ç, Bayramoğlu M (2022) One pot synthesis of graphene through microwave assisted liquid exfoliation of graphite in different solvents. Molecules 27:5027
[90] Li J, Wu J, Huang Z, Qi X, Zhong J (2019) Local conductivity of graphene oxide study by conductive atomic force microscope. J Appl Phys 126:215701
[91] Chlanda A, Walejewska E, Kowiorski K, Heljak M, Swieszkowski W, Lipińska L (2021) Investigation into morphological and electromechanical surface properties of reduced-graphene-oxide-loaded composite fibers for bone tissue engineering applications: a comprehensive nanoscale study using atomic force microscopy approach. Micron 146:103072
[92] Gao N, Cai Z, Chang G, He Y (2023) Non-invasive and wearable glucose biosensor based on gel electrolyte for detection of human sweat. J Mater Sci 58:890–901
[93] Trinh TTPNX, Quang DT, Tu TH, Dat NM, Linh VNP, Van Cuong L, Nghia LTT, Loan TT, Hang PT, Phuong NTL, Phong MT, Nam HM, Hieu NH (2019) Fabrication, characterization, and adsorption capacity for cadmium ions of graphene aerogels. Synthetic Metals 247:116–123
[94] Yadav KK, Wadhwa R, Khan N, Jha M (2021) Efficient metal-free supercapacitor based on graphene oxide derived from waste rice. Curr Res Green Sustain Chem 4:100075
[95] Anurag K, Kumar SR (2023) Scalable preparation of high-quality graphene by electrochemical exfoliation: effect of hydrogen peroxide addition. Bull Mater Sci 46:42
[96] Masrie M, Badaruddin SAM, Hussin MRM, Nor N, Joe J (2020) Rapid reduction of graphene oxide thin films on large-area silicon substrate. J Phys Conf Ser 1535:012027
[97] Tas M, Altin Y, CelikBedeloglu A (2019) Reduction of graphene oxide thin films using a stepwise thermal annealing assisted by l-ascorbic acid. Diam Relat Mater 92:242–247
[98] IEC, TS 62607-6-1:2020 (2020) Nanomanufacturing—key control characteristics—Part 6–1: graphene-based material—volume resistivity: four probe method. https://webstore.iec.ch/publication/32147. Accessed 1 Jul 2024
[99] Melios C, Huang N, Callegaro L, Centeno A, Cultrera A, Cordon A, Panchal V, Arnedo I, Redo-Sanchez A, Etayo D, Fernandez M, Lopez A, Rozhko S, Txoperena O, Zurutuza A, Kazakova O (2020) Towards standardisation of contact and contactless electrical measurements of CVD graphene at the macro-, micro- and nano-scale. Sci Rep 10:3223
[100] Okigawa Y, Kato R, Yamada T, Ishihara M, Hasegawa M (2015) Electrical properties and domain sizes of graphene films

synthesized by microwave plasma treatment under a low carbon concentration. Carbon 82:60–66
[101] Kulyk B, Carvalho AF, Fernandes AJS, Costa FM (2020) Millimeter sized graphene domains through in situ oxidation/reduction treatment of the copper substrate. Carbon 169:403–415
[102] IEC, TS 62607-6-3:2020 (2020) Nanomanufacturing—key control characteristics—Part 6–3: graphene-based material—domain size: substrate oxidation. https://cdn.standards.iteh.ai/samples/21466/172f0900d83d452e80ba57890dd8cbfd/IEC-TS-62607-6-3-2020.pdf. Accessed 1 Jul 2024

Publisher's Note Springer Nature remains neutral with regard to jurisdictional claims in published maps and institutional affiliations.